Mon. Not. R. Astron. Soc. **000**, 1–29 (2014) Printed 17 March 2015 (MN LATEX style file v2.2)

Methane and Ammonia in the near-infrared spectra of late T dwarfs

J. I. Canty[1⋆] P.W. Lucas[1] Sergei N. Yurchenko[2] Jonathan Tennyson[2]
S. K. Leggett[3] C. G. Tinney[4] H. R. A. Jones[1] Ben Burningham[1]
D. J. Pinfield[1] R. L. Smart[5]
[1] *Centre for Astrophysics Research, University of Hertfordshire, College Lane, Hatfield AL10 9AB, UK*
[2] *Department of Physics and Astronomy, University College London, London WC1E 6BT, UK*
[3] *Gemini Observatory, Northern Operations Center, 670 North A'ohoku Place, Hilo, HI 96720, USA*
[4] *Department of Astrophysics, School of Physics, University of New South Wales, Sydney, NSW 2052, Australia*
[5] *Istituto Nazionale di Astrofisica, Osservatorio Astrofisico di Torino, Strada Osservatorio 20, I-10025 Pino Torinese, Italy*

17 March 2015

ABSTRACT

Analysis of T dwarfs using model atmospheres has been hampered by the absence of reliable line lists for methane and ammonia. Newly computed high temperature line lists for both of these important molecules are now available, so it is timely to investigate the appearance of the various absorption features in T dwarfs in order to better understand their atmospheres and validate the new line lists. We present high quality R∼5000 Gemini/NIFS 1.0-2.4 μm spectra of the T8 standard 2MASS 0415-0935 and the T9 standard UGPS 0722-0540. We use these spectra to identify numerous methane and ammonia features not previously seen and we discuss the implications for our understanding of T dwarf atmospheres. Among our results, we find that ammonia is the dominant opacity source between ∼1.233-1.266 μm in UGPS 0722 0540, and we tentatively identify several absorption features in this wavelength range in the T9's spectrum which may be due entirely to ammonia opacity. Our results also suggest that water rather than methane is the dominant opacity source in the red half of the J-band of the T8 dwarf. Water appears to be the main absorber in this wavelength region in the T9 dwarf until ∼1.31 μm, when methane starts to dominate.

Key words: stars: atmospheres − stars: low-mass − stars: brown dwarfs.

1 INTRODUCTION

Amongst the first brown dwarf discoveries was a T dwarf (Oppenheimer et al. 1995). Since then, a large number of T dwarfs have been discovered in the local field using surveys such as 2MASS (Skrutskie et al. 2006), SDSS (York et al. 2000), UKIDSS (Lawrence et al. 2007), and now WISE (Wright et al. 2010). T dwarfs provide a new arena for studying atmospheric physics at T_{eff} cooler than stars but warmer than gas giant planets such as Jupiter. WISE has recently discovered the first Y dwarfs, objects with T_{eff} ∼275-450 K, and has tentatively identified ammonia opacity on the blue wing of the H-band flux peak (Cushing et al. 2011, hereafter C11). However, Y dwarfs are too faint for medium resolution spectroscopy of individual narrow molecular absorption features with instruments such as Gemini/NIFS (McGregor et al. 2003). We anticipate that the James Webb Space Telescope will provide an ideal platform for spectroscopy of Y dwarfs at a higher resolution than is currently possible.

The range of T_{eff} of late T dwarfs is uncertain, owing to the complicated atmospheric microphysics of these very cool objects and, until recently, the absence of good methane and ammonia line lists. Distance and temperature estimates based on model fits to near-infrared spectra are often found to be incorrect, in some instances by a factor of 2 in distance (Liu et al. 2011). Improved model atmospheres are essential in order to derive reliable temperatures, luminosities, and gravities for cold brown dwarfs, without recourse to time-consuming parallax measurements. This is a basic requirement in order to determine the substellar mass function in the local field, and to enable brown dwarfs to inform our understanding of the many warm gas giant exoplanets, which are hard to study in any detail.

In low resolution late T dwarf spectra, only broad and overlapping absorption bands of water and methane are

⋆ E-mail:j.canty2@herts.ac.uk

typically observed at 1.0-2.4 μm. Medium resolution spectroscopy with instruments such as NIFS resolves the bands into narrow features produced by blends of individual transition lines and detects other features such as blends of numerous weak ammonia lines across the near-infrared, as well as the temperature sensitive K I doublet at 1.18 μm and 1.24 μm. Bochanski et al. (2011), hereafter B11, have demonstrated this with the first medium resolution spectrum of a single object (the T9 standard UGPS 0722-0540, hereafter UGPS 0722), obtained with Magellan/FIRE (Simcoe et al. 2010) during a commissioning run. Our data for UGPS 0722 agree closely with the Magellan/FIRE data of B11 (see Figures 3, 7, and 10). We note that some molecular features have been resolved in the T6.5 dwarf Gliese 229B at lower resolutions (R$\sim$2400$-$2800) (Saumon et al. 2000).

Such data offer the opportunity to directly test the details of previously inadequate near-infrared model spectra. Saumon et al. (2012), hereafter S12, have recently published improved model atmospheres that incorporate a new high-temperature, synthetic ammonia line list (BYTe) (Yurchenko et al. 2011), and new calculations of collision-induced absorption of molecular hydrogen (H_2 CIA) (Richard et al. 2012). S12 also had access to an improved, though still incomplete, treatment of methane opacity (Freedman et al. 2008).

The ExoMol project (Tennyson & Yurchenko 2012) provides a database (www.exomol.com) of high temperature line lists for astronomical use. The database now includes a new high-temperature, synthetic methane line list (10to10) (Yurchenko & Tennyson 2014). Yurchenko & Tennyson (2014) used the 10to10 line list to re-identify a number of methane absorption features first identified in the $R \sim$1200 SpeX (Rayner et al. 2003) H-band spectrum of the T4.5 brown dwarf 2MASS J0559-1404 (Cushing et al. 2005). The 10to10 list has also been incorporated into the VSTAR model atmosphere code (Bailey & Kedziora-Chudczer 2012) and used to model the H- and K-band spectrum of 2MASS J0559-1404 (Yurchenko et al. 2014). The model spectrum is a significantly better fit to the brown dwarf spectrum than an earlier VSTAR model using a methane line list computed with the STDS (Wenger & Champion 1998) software. However, medium resolution spectra are needed to resolve individual features. It is therefore timely to provide a high quality set of medium resolution spectra to compare with the new generation of models.

In this paper, we examine the atmospheres of two late T dwarf standards by comparing absorption features in the near-infrared spectra of these objects with synthetic spectra and with absorption cross-sections of the most important gas-phase opacity sources at these wavelengths; H_2O, CH_4, and NH_3. We also conduct an analysis of the rotational-vibrational (ro-vibrational) transition lines responsible for the methane and ammonia absorption features in these objects' near-infrared spectra.

The structure of this paper is as follows. In Section 2 we describe how the T dwarfs were observed and how we extracted their spectra. Section 3 contains the results of our analysis of the CH_4 absorption features in the near-infrared spectra of the T dwarfs. Section 4 analyses the NH_3 absorption features in these objects. We discuss our results in Section 5. Our conclusions are made in Section 6.

2 OBSERVATIONS & DATA REDUCTION

Observations were made with the 8m Gemini Telescope at Gemini North on Mauna Kea, Hawaii, using the near-infrared integral field spectrograph (NIFS) (McGregor et al. 2003). Observations were made in the Z, J, H, and K passbands, (the Z passband includes the Y-band flux peak in brown dwarfs). The resolution in each passband was R$\sim$5000. The T8 standard 2MASS 0415-0935 (hereafter 2MASS 0415) was observed over four nights between 2010 September 30 and 2010 October 12. Observations of UGPS 0722 were made over seven nights between 2010 October 17 and 2012 October 29. Observations in the H and K passbands for UGPS 0722 were made using the Gemini ALTAIR adaptive optics system to improve the S/N ratio. Details of the observations and the physical properties of the two T dwarfs are shown in Tables 1 and 2 respectively.

Observations were made in an ABBA pattern to facilitate the removal of the sky background and dark current. Raw data in each waveband were reduced using the GEMINI/NIFS package within IRAF. The reduction was made in three steps.

(1) a baseline calibration to produce a reference file to determine the shift between the position of the data and the location of the image slices on the detector, a flat field file, a flat bad pixel mask file, a wavelength referenced arc file, and a file to correct for spatial distortion of the data;
(2) a telluric calibration reduction to produce a 1D spectrum of the standard star to be used for telluric calibration of the science data;
(3) a science data reduction to produce a 3D data cube which has been sky subtracted, flat fielded, cleaned of bad pixels, and telluric corrected.

The first two steps in the reduction process were completed by editing processing scripts supplied by the Gemini Observatory. The science reduction also largely followed a Gemini script. However, several additional steps were required to complete the reduction. In particular, any hydrogen absorption lines in the spectrum of the standard star chosen for the telluric calibration of each science spectrum had to be removed, the modified spectrum then being divided by the star's blackbody spectrum and normalised before being divided into the extracted 1D science object spectrum to correct the latter for telluric absorption features.

The spectra were extracted using an aperture size of 1.5 times the full width at half maximum (FWHM) of each object, as determined from the dispersed images.

Observations in the near-infrared are susceptible to contamination by telluric OH sky lines. For the fainter objects observed here, the flux in the sky lines often varied sufficiently during the exposures that the lines were poorly subtracted in the reduction. To remove these lines as well as cosmic ray strikes, bad pixels, and the general background, the data were processed using our own scripts to subtract the residual background along each column and interpolate across isolated pixels with highly anomalous counts. Care was taken to ensure that the scripts removed only noise features, using a comparison of the many image slices within each dispersed image to distinguish real features from noise.

The science spectra were corrected for the T dwarfs'

Table 1. T Dwarf Observations

Object	Observation period	Grating/centred at	Wavelength Range
2MASS 0415	2010 October 4	Z-band/1.05 μm	0.95-1.15 μm
	2010 October 12	J-band/1.25 μm	1.15-1.35 μm
	2010 October 1	H-band/1.6 μm	1.45-1.75 μm
	2010 September 30	K-band/2.14 μm	1.95-2.37 μm
UGPS 0722	2012 September 27 - 2012 September 30	Z-band/1.05 μm	0.95-1.15 μm
	2012 October 1 - 2012 October 29	J-band/1.25 μm	1.15-1.35 μm
	2011 December 11	H-band/1.6 μm	1.45-1.75 μm
	2010 October 17	K-band/2.14 μm	1.95-2.37 μm

Table 2. T Dwarf Physical Properties

	UGPS 0722	2MASS 0415
Spectral Type	T9 [1]	T8 [2]
T_{eff}	500 K[3],[8]	750 K [4]
v sin i	40±10 kms^{-1} [5]	33.5 kms^{-1} [6]
RV	46.9±2.5 kms^{-1} [5]	49.6 kms^{-1} [6]
Age	1-5 Gyr [5]	1-10 Gyr [2]
log g	4.39-4.90[7]	4.64-5.15[7]
Mass	10.7-25.8 M_J [7]	17.4-40.1 M_J [7]
Distance	4.12±0.04 pc[8]	5.71±0.05 pc[9]

[1]C11 [2] Burgasser et al. (2002) [3] Lucas et al. (2010)
[4] Saumon et al. (2007) [5] B11 [6] Zapatero Osorio et al. (2007)
[7] Dupuy & Kraus (2013) [8] Leggett et al. (2012)
[9] Dupuy & Liu (2012)

radial velocities using the IRAF task DOPCOR. The radial velocity for 2MASS 0415 was taken from Zapatero Osorio et al. (2007), that for UGPS 0722 from B11. Both T dwarf spectra were corrected for the heliocentric and barycentric velocity components of Earth using the IDL/AstroLib task BARYVEL. In the spectrum of UGPS 0722, we estimate the S/N ratio at the peaks of the Z-, J-, H-, and K-bands to be ∼250, 370, 300, and 80 respectively. B11's estimates for the corresponding values in their analysis of UGPS 0722 are ∼250, 350, 200, and 60. We note that Magellan/FIRE data split each passband into multiple orders which can cause more variation in the S/N ratio with wavelength. This is not the case with NIFS, where data are collected in separate observations in each passband. Our T dwarf spectra are shown in Figure 1

3 METHANE

In the following discussion, the terms CH_4 and methane refer to the main isotopologue of methane, $^{12}CH_4$. We examined a number of absorption features in the H-band of UGPS 0722, which we suspected may have been produced by the $^{13}CH_4$ isotopologue, but none of these features coincided with $^{13}CH_4$ lines in the HITRAN (Rothman et al. 2009) molecular spectroscopic database.

Carbon in the photospheres of early to mid L type brown dwarfs is predominantly found as carbon monoxide (CO) due to the molecule's high dissociation energy (Geballe et al. 2009). By spectral type L5, the photosphere is cool enough to allow the hydrogenation of CO to CH_4 (Noll et al. 2000). As the photosphere continues to cool, CH_4 becomes the dominant carbon-bearing species (Fegley & Lodders 1996).

We have used absorption cross-sections at 500 K and 750 K, derived from the 10to10 line list to identify methane absorption features in the near-infrared spectra of the two T dwarfs. Absorption cross-sections were calculated at zero-pressure and do not consider collisional broadening effects. At the highest resolutions, this could lead to differences between opacity plots and model spectra, but is not a concern at the resolution of our T dwarf spectra (Hill et al. 2013). These cross-sections were compared with cross-sections at the same temperatures for H_2O and NH_3, calculated respectively from the BT2 (Barber et al. 2006) and BYTe line lists. Each cross-section was scaled by the relative abundances of these molecules according to Figure 3 in Saumon et al. (2006). We have adopted the mole fractions of log −3.129 (H_2O), log −3.312 (CH_4), and log −4.907 (NH_3). The same values were used for the 500 K and 750 K opacity plots. We note that the molecular abundances along the profiles in Figure 3 in Saumon et al. (2006), and also in Figure 5 of Geballe et al. (2009) are constant with depth to ∼0.1 dex (except well below the photosphere). The abundance for NH_3 included non-equilibrium effects in the model atmosphere.

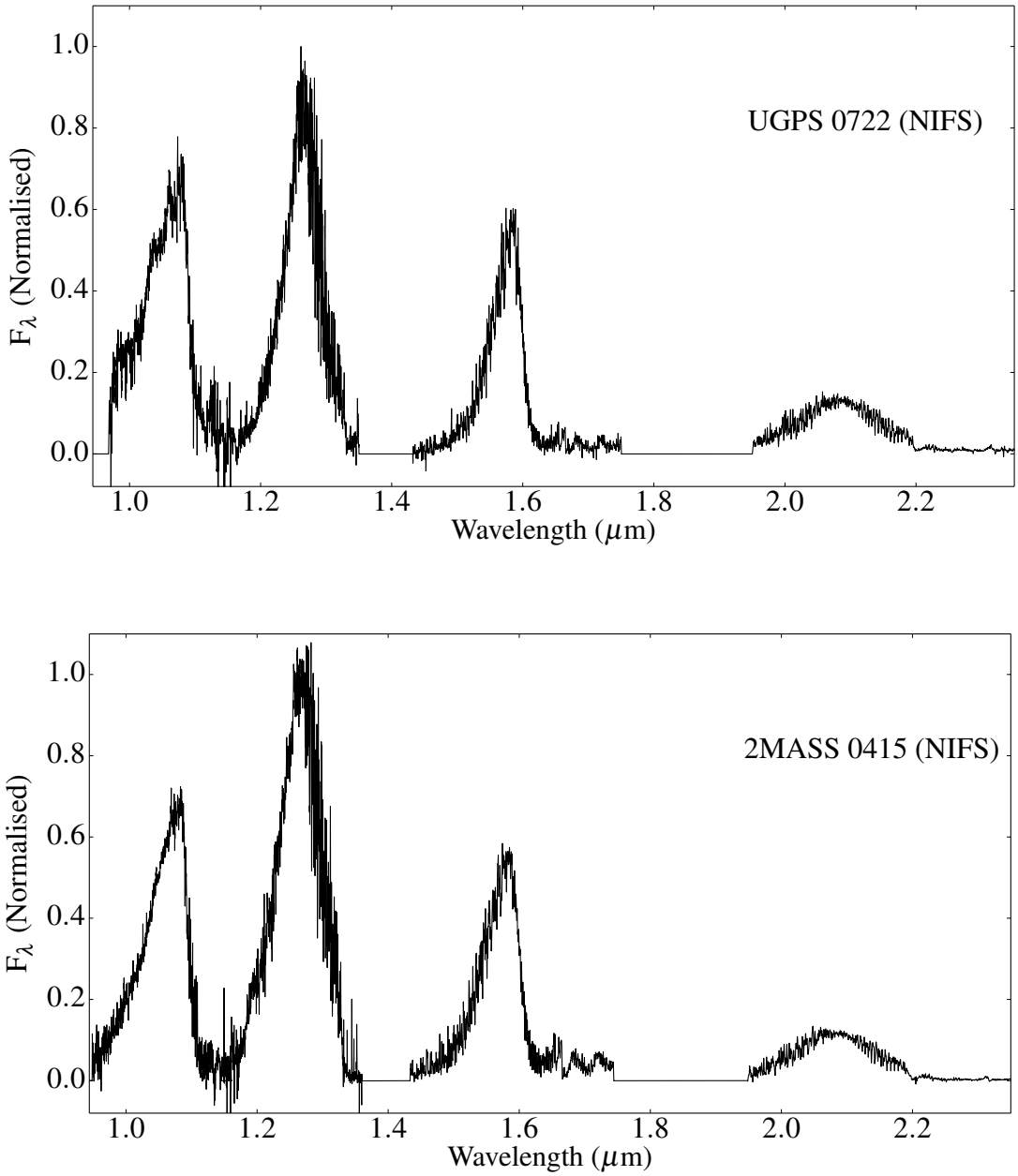

Figure 1. Top. The near-infrared spectrum of the T9 standard UGPS 0722. **Bottom.** The near-infrared spectrum of the T8 standard 2MASS 0415.

3.1 Ro-vibrational spectroscopy of non-linear molecules

CH_4 electric dipole transitions are due to changes in a manifold of rotational energies, ΔJ, superimposed on larger vibrational energy changes, $\Delta\nu$. In any particular waveband, R-branch (ΔJ= +1), Q-branch (ΔJ=0), and P-branch (ΔJ= −1) transitions form a sequence in wavelength. We have not detected electric quadrupole transitions from the O-branch (ΔJ= −2), and S-branch (ΔJ= +2) in our analysis of the T dwarf spectra.

If CH_4 was a simple harmonic oscillator, absorption features could only be produced by transitions between adjacent vibrational energy levels. As this is not the case, transitions involving $\Delta\nu = \pm2$, ±4, ±6,...etc. are possible. We show in Section 3.4 that the strongest features in the H-band absorption spectrum of CH_4 are produced by overtones.

Molecules may be classified according to their symmetry, and assigned to certain point groups. CH_4 is a tetrahedral molecule and belongs to the T_d point group. It has four fundamental vibrational modes or states, described by four quantum numbers. The modes and their properties are shown in Table 3.

It can be seen from Table 3 that three of the modes are degenerate. ν_2 is doubly degenerate, while ν_3 and ν_4

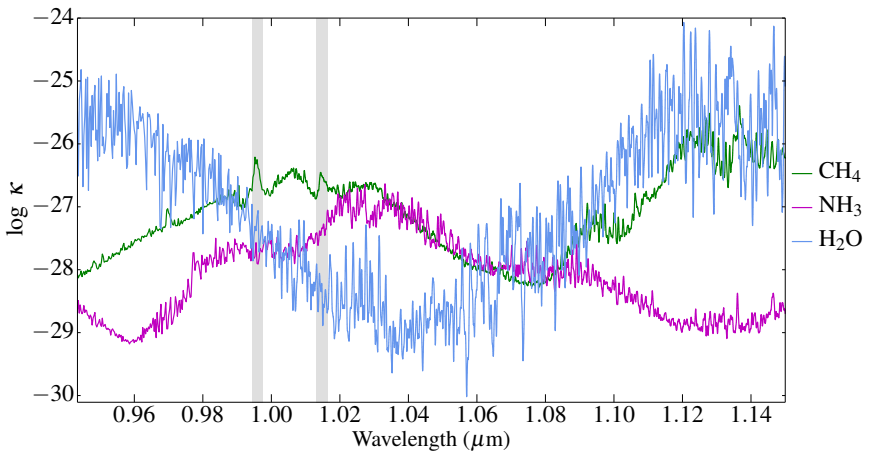

Figure 2. Molecular opacities in the Z-band. The graph shows the log of the scaled absorption cross-sections at 500 K for CH_4 (green), NH_3 (magenta) and H_2O (blue). By scaled, we mean that the cross-sections have been corrected for the relative molecular abundances expected for each molecule according to Figure 3 in Saumon et al. 2006. Methane opacity is the dominant opacity source between ∼0.995-1.032 μm where the continuum contains two prominent Q-branch regions (shaded). Cross-sections are measured in units of square centimetres per molecule (see Equation 4 in Hill et al. 2013). These units are used in all similar graphs in this paper.

Table 3. The Fundamental Vibrational Modes ($\Delta\nu = 1$) of Methane

Mode	Type	Wavenumber (cm^{-1})	Symmetry	Components
ν_1	Symmetric Stretch	2917	A_1	1
ν_2	Symmetric Bend	1534	E	2
ν_3	Asymmetric Stretch	3019	F_1	3
ν_4	Asymmetric Bend	1306	F_2	3

each have three components sharing the same energy. Note that the symmetric modes impart no motion to the carbon atom. In most cases, excited stretching states are stronger than excited bending states. In the H-band, for example, the strongest features belong to the $2\nu_3$ vibrational band, which is a stretching band.

3.2 The Z-Band

In the Z-band, CH_4 is the major opacity source between ∼0.995−1.032 μm, where the cross-section is marked by two Q-branch regions, centred at ∼0.9957 μm and ∼1.0152 μm (see Figure 2). We have not identified any methane features in the Z-band spectra of either T dwarf. The non-detection of the Q-branch CH_4 features can be attributed to the low flux level in the Z-band at these wavelengths.

3.3 The J-Band

There has been very little work done on intermediate resolution spectroscopy of T dwarfs. Up till now, we are only aware of one paper that has been published in this area, that by B11. By comparing their spectrum of UGPS 0722 with molecular line lists, B11 were able to identify absorption features due to H_2O and CH_4. They have also made the first confirmed detections of NH_3 opacity in the near-infrared spectrum of a T dwarf. While B11 used the BT2 and BYTe line lists we use in our analysis, they used an old CH_4 line list (Nassar & Bernath 2003), supplemented by the HITRAN 2008 database (Rothman et al. 2009).

Figure 3 shows the J-band spectra of UGPS 0722 and 2MASS 0415 and the corresponding CH_4 absorption cross-sections at 500 K and 750 K. The figure shows CH_4 opacity reducing with increasing wavelength over the width of the short side of the J-band flux peak. This decrease in opacity is particularly smooth in the 750 K cross-section. On the long side of the J-band flux peak, the opacity shown by both cross-sections increases, producing regular patterns of peaks, separated by ∼0.002 μm, from ∼1.30 - 1.33 μm.

B11 identified a number of blended CH_4 features on the short side of the J-band flux peak in the T dwarf's spectrum at 1.2390 μm, 1.2406 μm, 1.2439 μm, 1.2540 μm, 1.2578 μm, 1.2624 μm, 1.2635 μm, and 1.2661 μm. We have found absorption features at these wavelengths in the spectrum of UGPS 0722 (see Figure 5), but only the feature at 1.2540 μm corresponds to a peak in the CH_4 opacity (and a much stronger peak in ammonia opacity). CH_4 opacity between ∼1.235-1.270 μm is generally flat. While the mean CH_4 opacity is greater than the H_2O opacity in this region, in several places it is surpassed by peaks in the H_2O opacity. In fact, NH_3 is the main opacity source in this region and we find that the majority of these features can be attributed to ammonia opacity. (See Section 4.2 for a fuller discussion of ammonia opacity in the J-band spectra of these T dwarfs). In contrast, water is the major opacity source in the same region in the spectrum of 2MASS 0415 (see Figure 4).

B11 identified two possible CH_4/H_2O absorption fea-

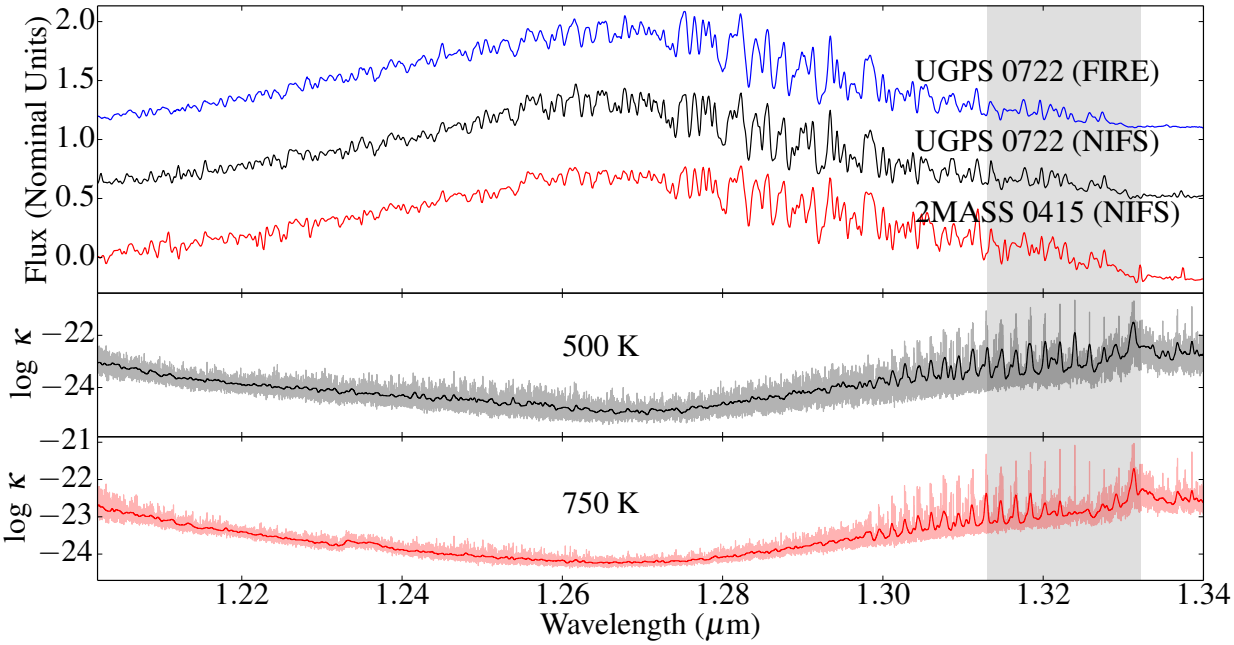

Figure 3. CH_4 absorption in the J-band spectra of 2MASS 0415 (red) and UGPS 0722 (black). The Magellan/FIRE spectrum of UGPS 0722 (blue) is shown for comparison. The middle and lower graphs show the unscaled absorption cross-sections at 500 K (black) and 750 K (red), smoothed to the same resolution as the T dwarf spectra, overplotted on the unsmoothed cross-sections. The shaded region indicates the Q-branch starting at ∼1.33 μm. (T dwarf spectra have been offset to aid identification of spectral features.)

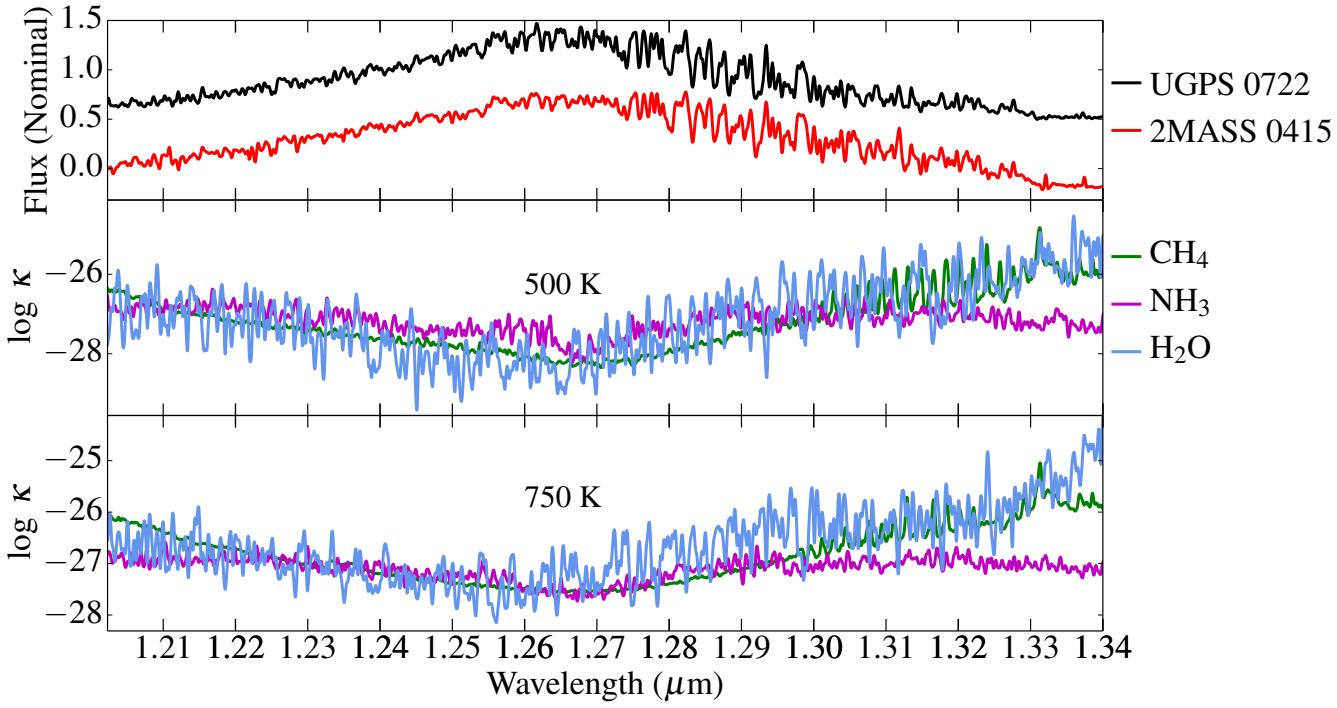

Figure 4. The increasing dominance of water opacity on the red side of the J band flux peak in late T dwarfs. The middle and lower graphs show the log of the scaled absorption cross-sections at 500 K and 750 K respectively for CH_4 (green), NH_3 (magenta) and H_2O (blue), smoothed to the same resolution as the T dwarf spectra.

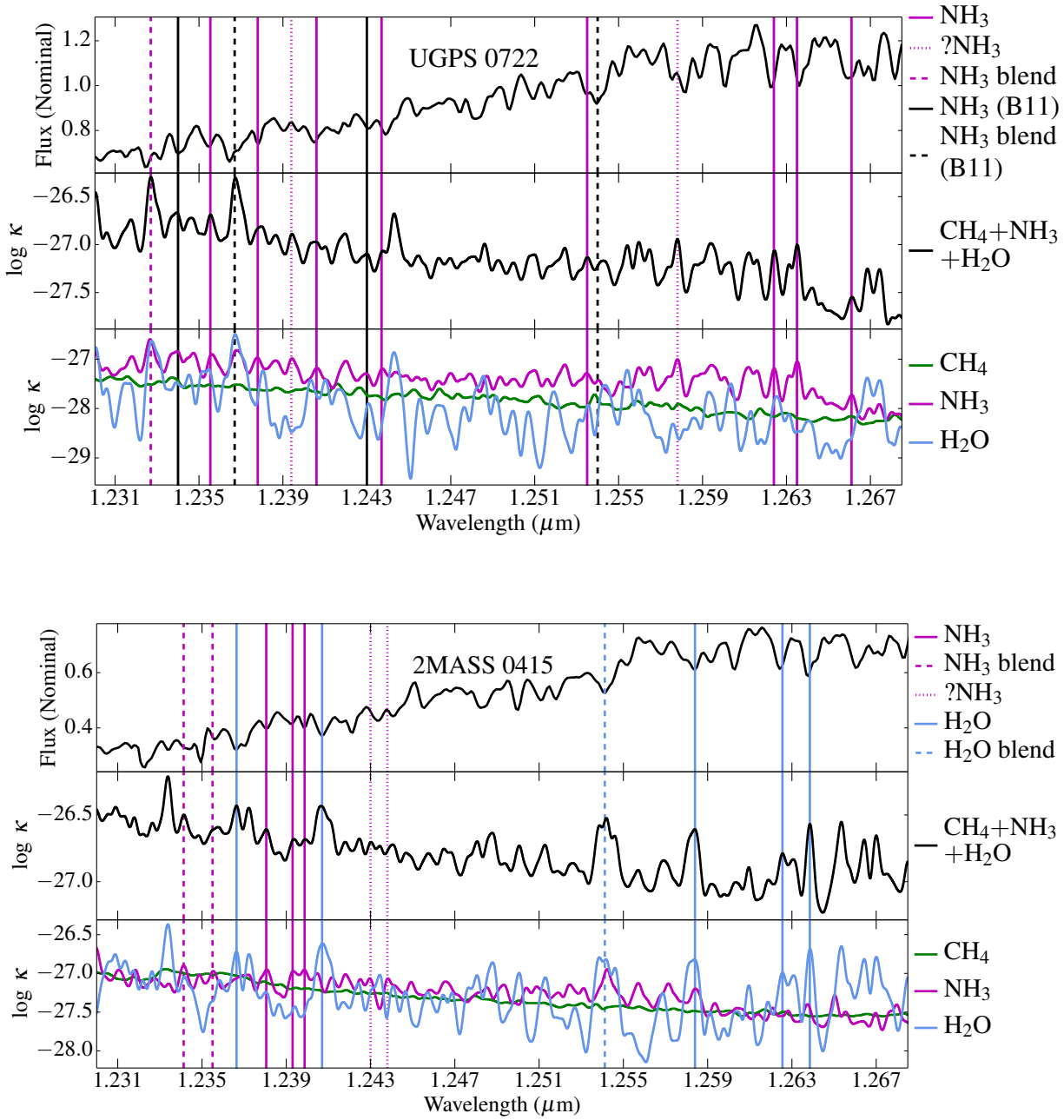

Figure 5. Opacities on the short side of the *J*-band flux peak. **Top.** Solid black lines identify NH_3 features detected by B11 in the spectrum of UGPS 0722. Dashed black lines are NH_3 blends identified by B11. Magenta lines are NH_3 features identified in this work. Most of the features appear to be due to ammonia opacity. The lower graph shows the log of the scaled absorption cross-sections at 500 K for CH_4 (green), NH_3 (magenta) and H_2O (blue), smoothed to the same resolution as the T dwarf spectrum. The middle graph is the sum of the scaled CH_4, NH_3 and H_2O opacities. **Bottom.** The same region in the spectrum of 2MASS 0415. Scaled opacity cross-sections have been made at 750 K. In this case, the dominant opacity source is H_2O.

tures either side of the peak in the spectrum of UGPS 0722 at ∼1.30 μm (see Figure 6). Neither cross-section shows a peak in CH_4 opacity at these wavelengths. We have determined that the feature at 1.2994 μm is due to water opacity, and that at 1.3004 μm is produced by a combination of water and ammonia opacity. B11 were more confident in identifying two CH_4+H_2O absorption features at 1.3043 μm and 1.3067 μm. While there is a peak in the CH_4 opacity at 1.3043 μm, we find that water is again the major opacity source at this wavelength, with a smaller contribution from NH_3 opacity. There is no corresponding peak in the CH_4 opacity at 1.3067 μm and we conclude that this is another water feature. A blended CH_4+H_2O absorption feature at 1.3097 μm is consistent with a peak in the CH_4 opacity, and a much stronger peak in water opacity. A CH_4 feature identified by B11 at 1.3112 μm is consistent with methane

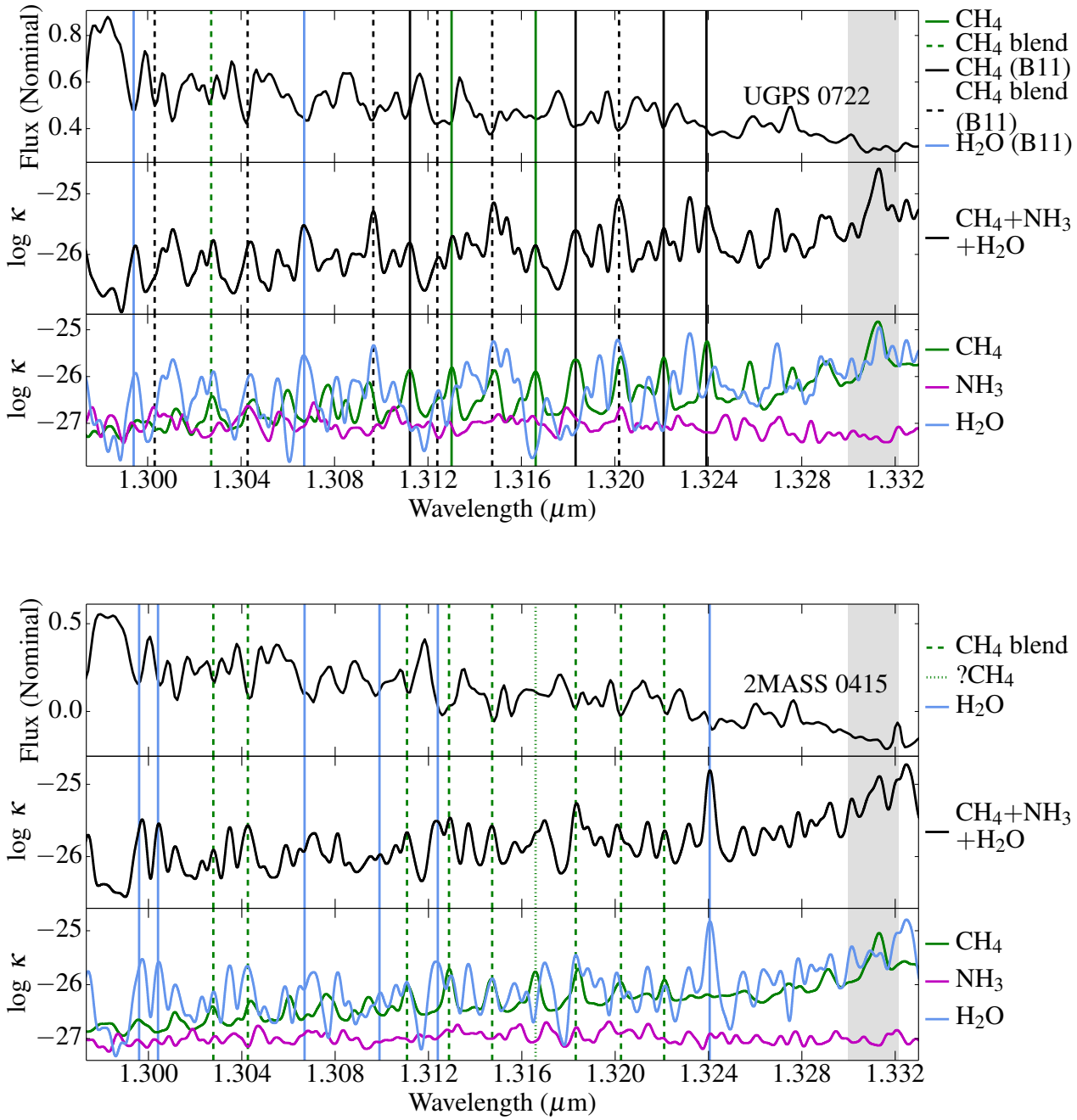

Figure 6. Top. CH_4 absorption features on the long side of the J-band flux peak in the spectrum of UGPS 0722 (see Table 4). Solid black lines are CH_4 features identified in B11. Solid green lines are CH_4 features identified in this work. Dashed black lines are mixed CH_4 features identified in B11. The dashed green line is a mixed CH_4 feature identified in this work. Solid blue lines indicate H_2O features previously identified as mixed CH_4 features. The lower graph shows the log of the absorption cross-sections at 500 K for CH_4 (green), NH_3 (magenta) and H_2O (blue), scaled by molecular abundances and smoothed to the same resolution as the T dwarf spectrum. The middle graph is the sum of the scaled CH_4, NH_3 and H_2O opacities at 500 K. Absorption features are produced by a blend of individual transition lines. **Bottom.** The same region in the spectrum of 2MASS 0415 showing the corresponding absorption features (see Table 4 again). Absorption cross-sections calculated at 750 K.

as the main opacity source. Opacities calculated using the 10to10 line list show that three CH_4 features at 1.3124 μm, 1.3148 μm, and 1.3202 μm are actually H_2O+CH_4 blends, while a CH_4+H_2O blend at 1.3183 μm is a "pure" methane feature. We can confirm the methane feature at 1.3221 μm. While CH_4 is the strongest opacity at 1.3284 μm, there is no peak in the CH_4 opacity corresponding to a previously identified CH_4 feature at this wavelength.

While the 10to10 line list has enabled us to correct previous mis-identifications of spectral features, it has also al-

lowed us to identify new CH_4 features at 1.3130 μm and 1.3166 μm. We have also identified a new H_2O+CH_4 feature at 1.3027 μm. See Figure 6, and Table 4.

These are late T dwarfs, and we would expect CH_4 absorption features to be prominent in both objects' spectra. However, in places the methane absorption in the T9 is deeper and/or broader than in the T8. For example, the absorption features at ∼1.3183 μm, 1.3202 μm and 1.3239 μm. That being said, we have identified fewer pure methane features in the J-band spectrum of UGPS 0722 than earlier studies, and find that a number of features previously identified as pure methane features are actually water features or water/methane blends. Additional water features are seen in the spectrum of 2MASS 0415 at 1.2334 μm, 1.2500 μm, and 1.2568 μm in Figure 5 and at 1.3012 μm, 1.3035 μm, 1.3081 μm, and 1.3255 μm in Figure 6. We have not marked these features as we are focussing here on methane and ammonia features. Nonetheless, it is clear that water is an important opacity source in the J-band spectra of these T dwarfs. In fact, our analysis suggests that water rather than methane is the dominant opacity source in the red half of the J-band in 2MASS 0415. In the case of UGPS 0722, water is the principal absorber until ∼1.31 μm, when methane opacity starts to dominate (see again Figure 4).

We have found that J-band absorption features in both T dwarfs' spectra are produced by R-branch line transitions belonging to the $\nu_2 + 2\nu_3$ vibrational band. Table 5 shows the changes in symmetries and ro-vibrational quantum numbers of the strongest line transitions for the CH_4 absorption features we have detected in the J-band spectra of UGPS 0722 and 2MASS 0415. Tables A1-A5 and B1-B6 showing the changes in symmetries and ro-vibrational quantum numbers of the strongest line transitions responsible, respectively, for the CH_4 and NH_3 absorption features we have detected in the near-infrared spectra of each T dwarf can be found in the electronic version of this paper.

3.4 The H-Band

The CH_4 absorption cross-sections at 500 K and 750 K show CH_4 opacity reaching a maximum on the long side of the H-band flux peak, producing regular patterns of peaks, separated by ∼0.002 μm, from ∼1.61-1.70 μm. The spectrum has a strong Q-branch composed of many transitions (see Figure 7). A comparison of the observed and modelled spectral energy distributions (SEDs) of three T7.5-8 dwarfs (Saumon et al. 2006; Saumon et al. 2007), ascribed a divergence in the model SEDs at 1.6-1.7 μm to an incomplete CH_4 line list. We expect that this discrepancy will be resolved with the inclusion of the 10to10 line list in model spectra.

B11 identified CH_4 absorption features at 1.6145 μm, 1.6168 μm, 1.6191 μm, 1.6213 μm, and 1.6258 μm. While CH_4 is the dominant opacity source in this wavelength range, the absorption cross-sections at 500 K show no peaks in the CH_4 opacity corresponding to these wavelengths. The same is true for the CH_4 absorption cross-sections made at 750 K, apart from the feature at 1.6258 μm (see Figures 8 and 9). However, the absorption features in the T dwarfs' spectra in this wavelength region are a clear extension of the pattern in absorption features at longer wavelengths in the data, and are only very slightly off-set from peaks in the CH_4 opacity. We suspected that these were methane features, and the failure of the opacity cross-sections to correspond with these features was most likely due to uncertainties in the 10to10 line list in this region. To examine this, the ExoMol group compiled a hybrid version of the 10to10 line list where some of the line positions, including lines in this region, were replaced with experimental values. This line list was then used to generate absorption intensities in the wavelength range 1.615-1.710 μm at T=500 K. The hybrid spectrum (not shown) produces peaks in the opacity which are in better agreement with the data, particularly at 1.6213 μm, and 1.6258 μm, indicating that the 10to10 features in this region are affected by deficiencies in ExoMol's theoretical model.

B11 did not identify CH_4 absorption features longward of 1.6354 μm. We have identified numerous CH_4 absorption features either side of the CH_4 Q-branch starting at ∼1.6650 μm. See Figure 8 and Table 6. In this region of the H-band, the CH_4 absorption cross-sections are ∼2 magnitudes stronger than other opacity sources, and all the features we have identified are "pure" CH_4 absorption features.

While the J-band absorption features we observed are from the R-branch, H-band absorption features in both T dwarfs are produced by ro-vibrational transitions in the R-, P-, and Q-branches. We did not identify isolated Q-branch absorption features. Instead, we note that the cluster of transition lines forming the Q-branch correspond to broad absorption troughs in the T dwarfs' spectra between ∼1.6651-1.6682 μm. These and the identified absorption features in 2MASS 0415 and UGPS 0722 belong to the $2\nu_3$ vibrational band. We consider that the pattern of strong peaks in the methane opacity in the H-band is most likely due to the $2\nu_3$ band being an allowed asymmetric stretching band with a non-zero dipole moment, in contrast, for example, to the $2\nu_1$ stretching band, which is also an overtone. While the features at 1.6976 μm and 1.7010 μm are largely due to P-branch transitions, each feature does contain an R-branch transition line. The R-branch lines have a similar intensity to the P-branch transition lines and belong to the $\nu_2+\nu_3+\nu_4$ vibrational band (1.6976 μm) and $\nu_1+\nu_3$ vibrational band (1.7010 μm). We consider it likely that these two lines are outlying members of the next set of R-branch transition lines.

3.5 The K-Band

The CH_4 absorption cross-sections show CH_4 opacity increasing with increasing wavelength over the long side of the K-band flux peak, reaching a maximum at ∼2.20 μm (see Figure 10). The absorption cross-sections clearly show the Q-branch transitions centred at ∼2.20 μm.

B11 detected a number of absorption features between ∼2.14 μm and ∼2.18 μm. Using the high quality of the Gemini/NIFS spectra and the greater accuracy of the 10to10 line list we have identified a number of new absorption features within this range (see Figure 11 and Table 7). Note that the features centred at ∼2.1278 μm and at ∼2.1429 μm are actually due to multiple peaks in the methane opacity which at this resolution (R∼5000) are marginally resolved.

The peak in the T dwarfs' K-band flux at ∼2.06 μm coincides with the start of increasing CH_4 opacity (see Figure 10). The continuum opacity of H_2 CIA is very high throughout the K-band [S12] and this will tend to veil narrow molecular features. H_2 CIA is produced by ro-vibrational transi-

Table 4. CH_4 Absorption Features in the J Band Spectra of Late T Dwarfs (see Figure 6)

Source	λ (μm)	Opacity Source (B11)	Opacity Source (500 K/750 K)	Absorption feature in UGPS 0722	Absorption feature in 2MASS 0415
B11	1.2994	CH_4(?)+H_2O	H_2O/H_2O	Yes	Yes
B11	1.3004	CH_4(?)+H_2O	(NH_3+H_2O)/H_2O	Yes	Yes
This work	1.3027	—	(H_2O+CH_4)/(H_2O+CH_4)	Yes	Yes
B11	1.3043	CH_4+H_2O	(H_2O+CH_4+NH_3)/(H_2O+CH_4)	Yes	Yes
B11	1.3067	CH_4+H_2O	H_2O/H_2O	Yes	Yes
B11	1.3097	CH_4+H_2O	(H_2O+CH_4)/H_2O	Yes	Yes
B11	1.3112	CH_4	CH_4/(H_2O+CH_4)	Yes	Yes
B11	1.3124	CH_4	(H_2O+CH_4)/H_2O	Yes	Yes
This work	1.3130	—	CH_4/(CH_4+H_2O)	Yes	Yes
B11	1.3148	CH_4	(H_2O+CH_4)/(H_2O+CH_4)	Yes	Yes
This work	1.3166	—	CH_4/CH_4	Yes	No(?)
B11	1.3183	CH_4+H_2O	CH_4/(H_2O+CH_4)	Yes	Yes
B11	1.3202	CH_4	(H_2O+CH_4)/(H_2O+CH_4)	Yes	Yes
B11	1.3221	CH_4	CH_4/(CH_4+H_2O)	Yes	Yes
B11	1.3239	CH_4+H_2O	CH_4/H_2O	Yes	Yes

In tables 4, 6, and 7, R-, Q-, and P-branch methane features are highlighted in red, grey, and blue respectively. Non-shaded regions are features produced by other opacity sources, which had previously been identified as due to methane or methane blends.

Table 5. R-branch ro-vibrational transition lines responsible for the CH_4 absorption features in the J band spectra of UGPS 0722 and 2MASS 0415 (shaded). Intensities were calculated using Equation 7 in Hill et al. 2013.

λ (μm)	Intensity (cm molecule^{-1})	$\Delta\Gamma$	ΔJ	$\Delta\nu_2$	ΔL2	$\Delta\nu_3$	ΔL3	ΔM3
1.3111927	1.94E-23	$A_1 \rightarrow A_2$	$10 \rightarrow 11$	$0 \rightarrow 1$	$0 \rightarrow 1$	$0 \rightarrow 2$	$0 \rightarrow 2$	$0 \rightarrow 1$
	1.38E-23	$A_1 \rightarrow A_2$	$10 \rightarrow 11$	$0 \rightarrow 1$	$0 \rightarrow 1$	$0 \rightarrow 2$	$0 \rightarrow 2$	$0 \rightarrow 1$
1.3128914	3.59E-23	$A_1 \rightarrow A_2$	$9 \rightarrow 10$	$0 \rightarrow 1$	$0 \rightarrow 1$	$0 \rightarrow 2$	$0 \rightarrow 2$	$0 \rightarrow 1$
	2.32E-23	$A_1 \rightarrow A_2$	$9 \rightarrow 10$	$0 \rightarrow 1$	$0 \rightarrow 1$	$0 \rightarrow 2$	$0 \rightarrow 2$	$0 \rightarrow 1$
1.3166163	6.50E-23	$A_2 \rightarrow A_1$	$7 \rightarrow 8$	$0 \rightarrow 1$	$0 \rightarrow 1$	$0 \rightarrow 2$	$0 \rightarrow 2$	$0 \rightarrow 1$
	3.54E-23	$A_2 \rightarrow A_1$	$7 \rightarrow 8$	$0 \rightarrow 1$	$0 \rightarrow 1$	$0 \rightarrow 2$	$0 \rightarrow 2$	$0 \rightarrow 1$
1.3184149	7.76E-23	$F_1 \rightarrow F_2$	$6 \rightarrow 7$	$0 \rightarrow 1$	$0 \rightarrow 1$	$0 \rightarrow 2$	$0 \rightarrow 2$	$0 \rightarrow 1$
	3.94E-23	$F_1 \rightarrow F_2$	$6 \rightarrow 7$	$0 \rightarrow 1$	$0 \rightarrow 1$	$0 \rightarrow 2$	$0 \rightarrow 2$	$0 \rightarrow 1$
1.3184160	7.66E-23	$A_1 \rightarrow A_2$	$6 \rightarrow 7$	$0 \rightarrow 1$	$0 \rightarrow 1$	$0 \rightarrow 2$	$0 \rightarrow 2$	$0 \rightarrow 1$
	3.89E-23	$A_1 \rightarrow A_2$	$6 \rightarrow 7$	$0 \rightarrow 1$	$0 \rightarrow 1$	$0 \rightarrow 2$	$0 \rightarrow 2$	$0 \rightarrow 1$
1.3184211	7.48E-23	$F_2 \rightarrow F_1$	$6 \rightarrow 7$	$0 \rightarrow 1$	$0 \rightarrow 1$	$0 \rightarrow 2$	$0 \rightarrow 2$	$0 \rightarrow 1$
	3.80E-23	$F_2 \rightarrow F_1$	$6 \rightarrow 7$	$0 \rightarrow 1$	$0 \rightarrow 1$	$0 \rightarrow 2$	$0 \rightarrow 2$	$0 \rightarrow 1$
1.3184622	7.26E-23	E $\rightarrow$ E	$6 \rightarrow 7$	$0 \rightarrow 1$	$0 \rightarrow 1$	$0 \rightarrow 2$	$0 \rightarrow 2$	$0 \rightarrow 1$
	3.69E-23	E $\rightarrow$ E	$6 \rightarrow 7$	$0 \rightarrow 1$	$0 \rightarrow 1$	$0 \rightarrow 2$	$0 \rightarrow 2$	$0 \rightarrow 1$
1.3184644	6.57E-23	$F_2 \rightarrow F_1$	$6 \rightarrow 7$	$0 \rightarrow 1$	$0 \rightarrow 1$	$0 \rightarrow 2$	$0 \rightarrow 2$	$0 \rightarrow 1$
	3.33E-23	$F_2 \rightarrow F_1$	$6 \rightarrow 7$	$0 \rightarrow 1$	$0 \rightarrow 1$	$0 \rightarrow 2$	$0 \rightarrow 2$	$0 \rightarrow 1$
1.3184738	6.14E-23	$A_2 \rightarrow A_1$	$6 \rightarrow 7$	$0 \rightarrow 1$	$0 \rightarrow 1$	$0 \rightarrow 2$	$0 \rightarrow 2$	$0 \rightarrow 1$
	3.12E-23	$A_2 \rightarrow A_1$	$6 \rightarrow 7$	$0 \rightarrow 1$	$0 \rightarrow 1$	$0 \rightarrow 2$	$0 \rightarrow 2$	$0 \rightarrow 1$
1.3220974	1.54E-22	$A_1 \rightarrow A_2$	$4 \rightarrow 5$	$0 \rightarrow 1$	$0 \rightarrow 1$	$0 \rightarrow 2$	$0 \rightarrow 2$	$0 \rightarrow 1$
	7.00E-23	$A_1 \rightarrow A_2$	$4 \rightarrow 5$	$0 \rightarrow 1$	$0 \rightarrow 1$	$0 \rightarrow 2$	$0 \rightarrow 2$	$0 \rightarrow 1$
1.3220991	1.17E-22	$F_1 \rightarrow F_2$	$4 \rightarrow 5$	$0 \rightarrow 1$	$0 \rightarrow 1$	$0 \rightarrow 2$	$0 \rightarrow 2$	$0 \rightarrow 1$
	5.31E-23	$F_1 \rightarrow F_2$	$4 \rightarrow 5$	$0 \rightarrow 1$	$0 \rightarrow 1$	$0 \rightarrow 2$	$0 \rightarrow 2$	$0 \rightarrow 1$
1.3221013	1.01E-22	$F_2 \rightarrow F_1$	$4 \rightarrow 5$	$0 \rightarrow 1$	$0 \rightarrow 1$	$0 \rightarrow 2$	$0 \rightarrow 2$	$0 \rightarrow 1$
	4.59E-23	$F_2 \rightarrow F_1$	$4 \rightarrow 5$	$0 \rightarrow 1$	$0 \rightarrow 1$	$0 \rightarrow 2$	$0 \rightarrow 2$	$0 \rightarrow 1$
1.3221177	1.32E-22	E $\rightarrow$ E	$4 \rightarrow 5$	$0 \rightarrow 1$	$0 \rightarrow 1$	$0 \rightarrow 2$	$0 \rightarrow 2$	$0 \rightarrow 1$
	6.00E-23	E $\rightarrow$ E	$4 \rightarrow 5$	$0 \rightarrow 1$	$0 \rightarrow 1$	$0 \rightarrow 2$	$0 \rightarrow 2$	$0 \rightarrow 1$
1.3239472	1.47E-22	$F_1 \rightarrow F_2$	$3 \rightarrow 4$	$0 \rightarrow 1$	$0 \rightarrow 1$	$0 \rightarrow 2$	$0 \rightarrow 2$	$0 \rightarrow 1$
	6.40E-23	$F_1 \rightarrow F_2$	$3 \rightarrow 4$	$0 \rightarrow 1$	$0 \rightarrow 1$	$0 \rightarrow 2$	$0 \rightarrow 2$	$0 \rightarrow 1$
1.3239478	1.88E-22	$F_2 \rightarrow F_1$	$3 \rightarrow 4$	$0 \rightarrow 1$	$0 \rightarrow 1$	$0 \rightarrow 2$	$0 \rightarrow 2$	$0 \rightarrow 1$
	8.20E-23	$F_2 \rightarrow F_1$	$3 \rightarrow 4$	$0 \rightarrow 1$	$0 \rightarrow 1$	$0 \rightarrow 2$	$0 \rightarrow 2$	$0 \rightarrow 1$
1.3239481	2.02E-22	$A_2 \rightarrow A_1$	$3 \rightarrow 4$	$0 \rightarrow 1$	$0 \rightarrow 1$	$0 \rightarrow 2$	$0 \rightarrow 2$	$0 \rightarrow 1$
	8.80E-23	$A_2 \rightarrow A_1$	$3 \rightarrow 4$	$0 \rightarrow 1$	$0 \rightarrow 1$	$0 \rightarrow 2$	$0 \rightarrow 2$	$0 \rightarrow 1$

$\Delta\Gamma$, ΔJ, and $\Delta\nu$ describe the changes in symmetry, rotational, and vibrational energy level between initial and final states.

tions in H_2 molecules, forming a series of bands corresponding to $\Delta\nu$=0, 1, 2, 3, etc. [S12]. The $\Delta\nu$=1 band is centred at $\sim$0.42 μm^{-1} ($\sim$2.4 μm). The roles played by these mechanisms in the K-band spectra of late T dwarfs will be clearer once the 10to10 line list is included in model atmospheres.

The shape of the K-band continuum is also affected by metallicity, but model fits to the SED and spectrum of UGPS 0722, combined with its small space motion, indicate that it is a young object and therefore low metallicity is

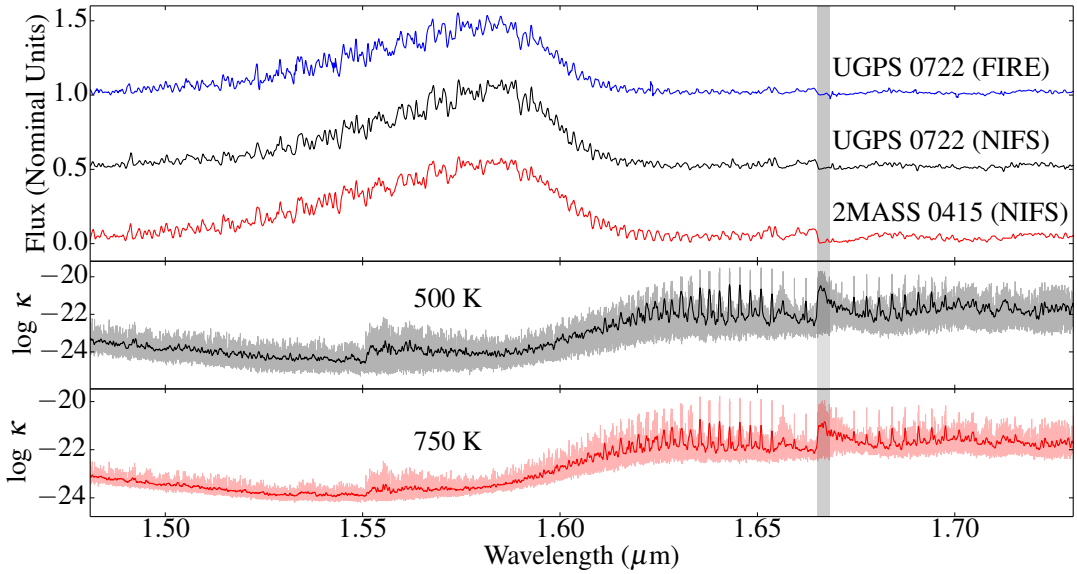

Figure 7. CH_4 absorption in the *H*-band spectra of 2MASS 0415 (red), UGPS 0722 (black), and the Magellan/FIRE spectrum of UGPS 0722 (blue). The shaded region indicates the Q-branch starting at ∼1.665 μm. The centre and lower graphs contains the cross-sections as described in Figure 3. (T dwarf spectra have been offset to aid identification of spectral features.)

Table 6. CH_4 Absorption Features in the *H* Band Spectra of Late T Dwarfs (see Figures 8 and 9)

Source	λ (μm)	Opacity Source (B11)	Opacity Source (500 K/750 K)	Absorption feature in UGPS 0722	Absorption feature in 2MASS 0415
B11	1.6145	CH_4	CH_4(?)/CH_4(?)	Yes	Yes
B11	1.6168	CH_4	CH_4(?)/CH_4(?)	Yes	Yes
B11	1.6191	CH_4	CH_4(?)/CH_4(?)	Yes	Yes
B11	1.6213	CH_4	CH_4(?)/CH_4(?)	Yes	Yes
B11	1.6236	CH_4	CH_4/CH_4	Yes	Yes
B11	1.6258	CH_4	CH_4(?)/CH_4	Yes	Yes
B11	1.6282	CH_4	CH_4/CH_4	Yes	Yes
B11	1.6307	CH_4	CH_4/CH_4	Yes	Yes
B11	1.6332	CH_4	CH_4/CH_4	Yes	Yes
B11	1.6354	CH_4	CH_4/CH_4	Yes	Yes
This work	1.6378	—	CH_4/CH_4	Yes	Yes
This work	1.6404	—	CH_4/CH_4	Yes	Yes
This work	1.6430	—	CH_4/CH_4	Yes	Yes
This work	1.6456	—	CH_4/CH_4	Yes	Yes
This work	1.6482	—	CH_4/CH_4	Yes	Yes
This work	1.6509	—	CH_4/CH_4	Yes	Yes
This work	1.6537	—	CH_4/CH_4	Yes	Yes
This work	1.6565	—	CH_4/CH_4	Yes	Yes
This work	1.6623	—	CH_4/(CH_4+H_2O)	Yes	Yes
This work	∼(1.6651→1.6682)	—	CH_4/CH_4	Yes	Yes
This work	1.6776	—	CH_4/CH_4	Yes	Yes
This work	1.6808	—	CH_4/CH_4	Yes	Yes
This work	1.6840	—	CH_4/CH_4	Yes	Yes
This work	1.6874	—	CH_4/CH_4	Yes	Yes
This work	1.6907	—	CH_4/CH_4	Yes	Yes
This work	1.6941	—	CH_4/CH_4	Yes	Yes
This work	1.6976	—	CH_4/CH_4	Yes	Yes
This work	1.7010	—	CH_4/CH_4	Yes	Yes

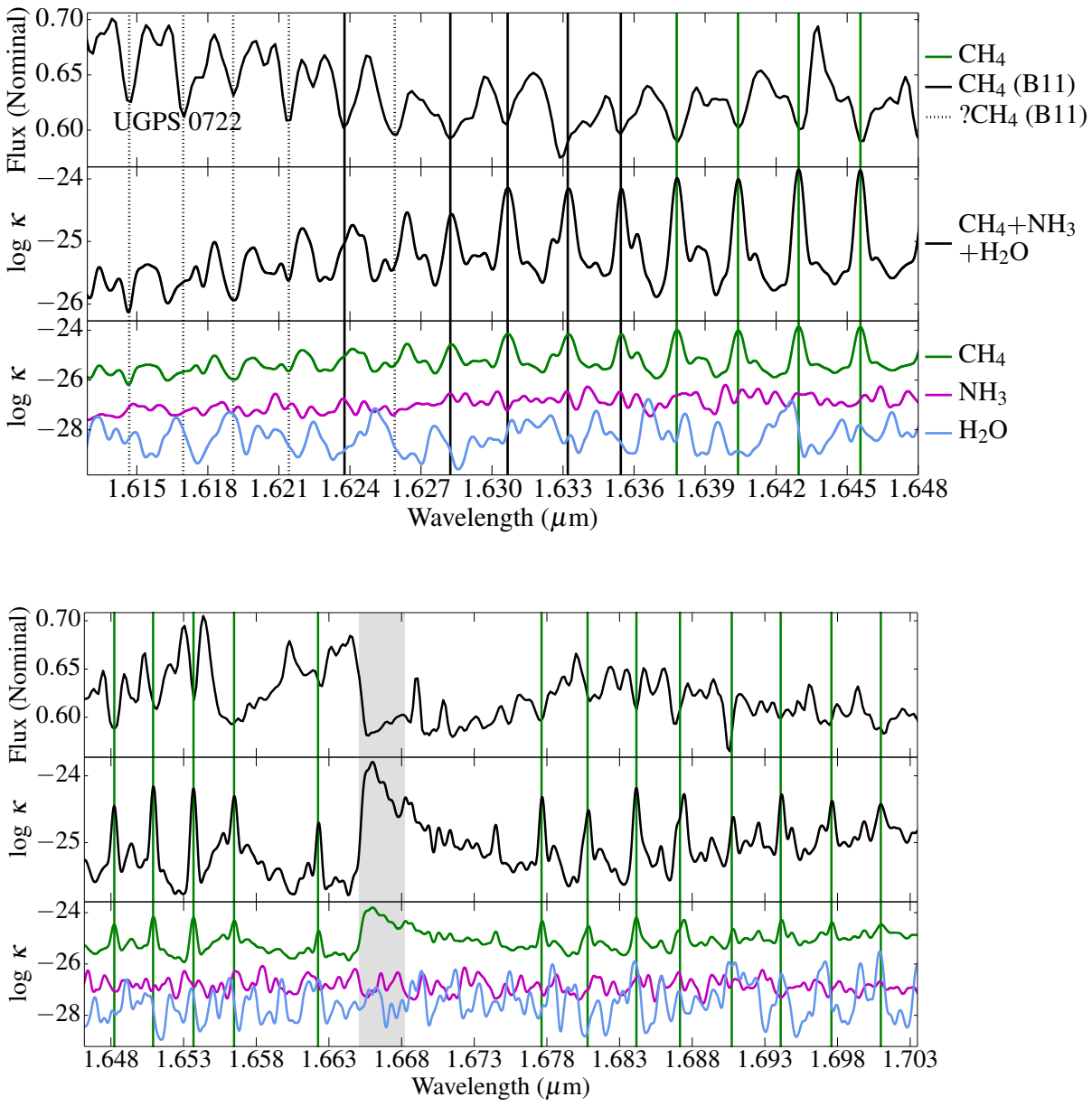

Figure 8. CH_4 absorption features in the H-band spectrum of UGPS 0722 (see Table 6). A large number of new methane features are detected (green lines) and several previously identified features are recovered (solid black lines). The black dotted lines are the locations of features which B11 identified as CH_4 absorption features but which do not correspond to peaks in the CH_4 opacity. The proximity of the features to peaks in the CH_4 opacity suggest that they are methane features. (See the text for more discussion of these features). The shaded region is the Q-branch centred at ∼1.665 μm. Other features are as those described in Figure 6.

unlikely (Leggett et al. 2012; Morley et al. 2012, hereafter M12).

In T dwarfs, the K-band flux weakens with increasing spectral type, i.e. decreasing temperature. H_2 CIA is dependent on pressure (surface gravity) rather than temperature. On the other hand, methane absorption becomes stronger as the temperature drops. It is possible that methane absorption is sufficiently strong on its own to completely suppress the K-band in this region. For example, the Q-branch peak transition at ∼2.20 μm is an order of magnitude stronger than most of the transitions responsible for the absorption features detected by B11 and us. The Q-branch peak transition at ∼2.32 μm (not shown) is an order of magnitude stronger still.

All the identified absorption features in UGPS 0722 and 2MASS 0415 arise from the $\nu_2 + \nu_3$ vibrational band. As with the J-band, these are all R-branch transitions.

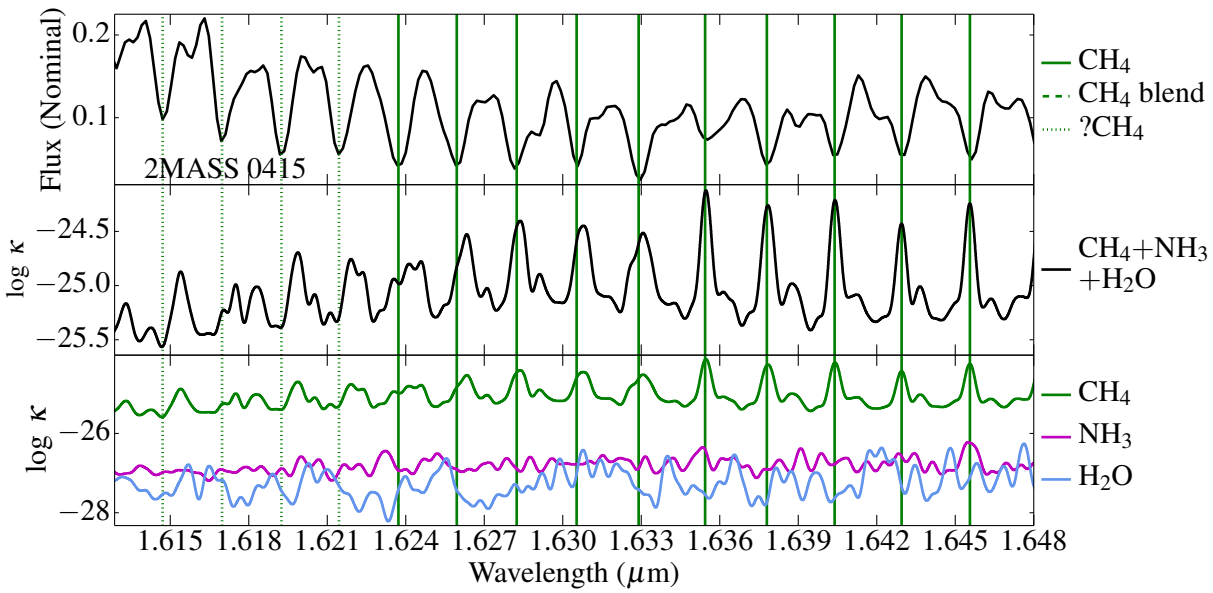

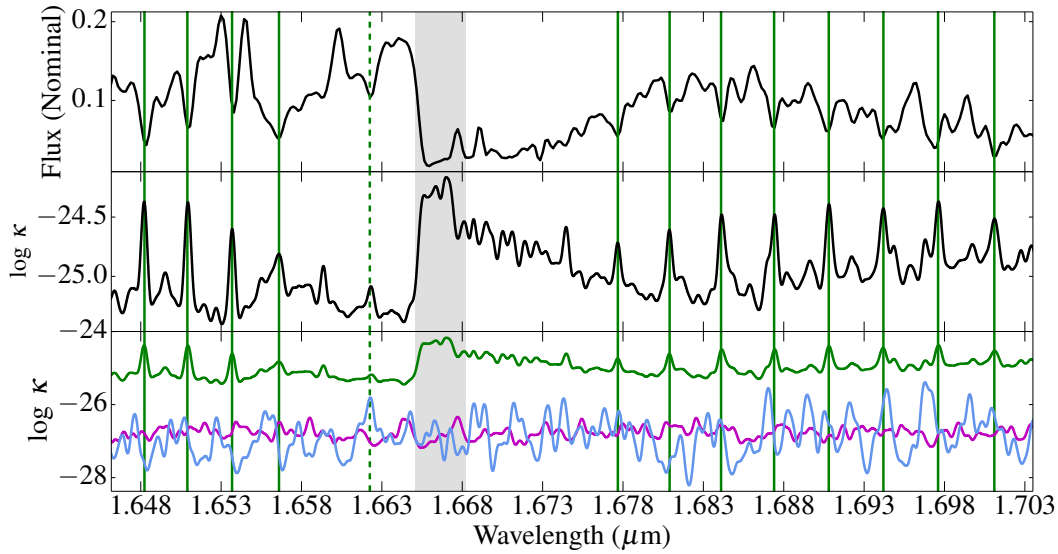

Figure 9. CH_4 absorption features in the H-band spectrum of 2MASS 0415 (see Table 6).

4 AMMONIA

In the following discussion, the terms NH_3 and ammonia refer to the main isotopologue of ammonia, $^{14}NH_3$. The conversion of N_2 into NH_3 occurs at T_{eff} ∼800 K [S12]. Bands of NH_3 opacity are first seen in the mid-infrared spectra of T2 dwarfs (Cushing et al. 2006), while the first unequivocal detection of NH_3 opacity in brown dwarfs was made in the mid-infrared spectra of the T dwarf binary ϵ Indi Bab (T1+T6) (Roellig et al. 2004; Mainzer et al. 2007). Features in low resolution near-infrared spectra of late T dwarfs and the recently discovered Y dwarfs have been attributed to weak bands of NH_3 opacity (Delorme et al. 2008; C11), but the first confirmed identification of ammonia features in the near-infrared spectrum of a late T dwarf was made by B11 using medium resolution spectra. This discovery has been significant in justifying the Y spectral class. Indeed, as we observed in Section 3.3, B11 may have underestimated the number of ammonia features in the J-band of UGPS 0722. By comparing synthetic spectra derived from full model atmosphere calculations with and without NH_3 opacity with the Magellan/FIRE spectrum of UGPS 0722 in B11, S12 were able to identify a number of new NH_3 absorption features. We have applied the technique described in S12 to the Gemini/NIFS spectra of 2MASS 0415 and UGPS 0722. The synthetic spectra were produced with solar metallicity and log g =4.25. Non-equilibrium chemistry was assumed, with eddy diffusion constant K_{zz}=10^4 cm^2 s^{-1}. Separate models were produced at 750 K and 500 K, the respective effective temperatures of the T8 and T9 objects. The models included

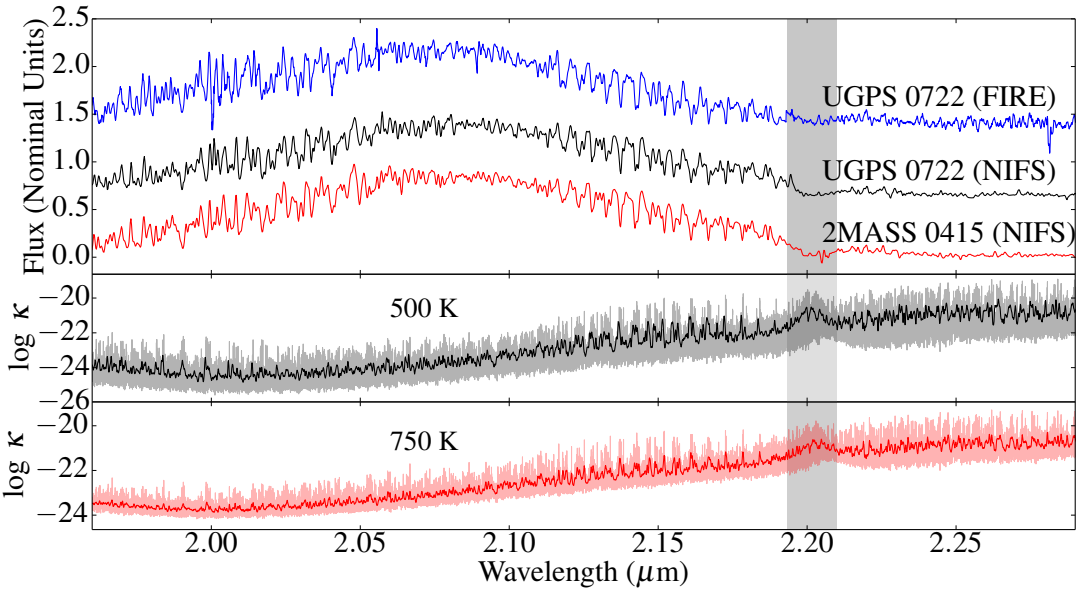

Figure 10. CH_4 absorption in the K-band spectra of 2MASS 0415 (red), UGPS 0722 (black), and the Magellan/FIRE spectrum of UGPS 0722 (blue). The shaded region indicates the Q-branch transitions centred at ∼2.20 μm. The lower graphs contains the cross-sections as described in Figure 3. (T dwarf spectra have been offset to aid identification of spectral features.)

the most recent calculations of all major opacity sources, except the 10to10 line list. With that caveat in mind, with the possible exception of regions where methane is the dominant opacity source, the model spectra should appear similar to the T dwarf spectra. It is also useful to have spectra from two dwarfs of successive spectral types since absorption features missing in the spectrum of one T dwarf, may be present in the spectrum of the other.

By comparing the T dwarf spectra with the S12 model spectra and the scaled cross-sections for CH_4, H_2O, and NH_3, we have been able to identify a number of new ammonia features in the near-infrared spectra of our T dwarfs (see Figures 13 − 18, and Tables 8 − 10).

In order to be confident in identifying an absorption feature, the shape of the S12 model spectra with and without NH_3 opacity should appear different, not simply in amplitude. In places, peaks in the NH_3 opacity do not coincide exactly with absorption troughs in the science spectrum. In these cases, we identify an ammonia feature at the wavelength of the peak in the NH_3 opacity when the science spectrum at this wavelength appears similar to the model spectrum with NH_3 opacity, e.g., the feature at 1.5240 μm in the spectrum of UGPS 0722 (see Figure 15). In a number of cases, features are predicted by the model spectra at 500 K and/or 750 K but are not found in the respective data. These results are also shown in Tables 8, 9, and 10.

4.1 The Z-Band

In the Z-band, the S12 models predict NH_3 opacity only between 1.005 μm and 1.074 μm. Across most of this wavelength range the S12 model spectra differ only in amplitude. Only at 1.0256 μm do we find a slight variation in structure between the two models, corresponding to a peak in NH_3 opacity and weak absorption features in both T dwarfs. However, the detection is weak, and we cannot say with confidence that we have found any evidence of NH_3 absorption features in the Z-band.

4.2 The J-Band

The scaled opacity cross-sections at 500 K show peaks in the NH_3 opacity between ∼1.210 μm and ∼1.276 μm. We compared these cross-sections with the S12 synthetic spectra at 500 K and identified a number of features between ∼1.2250−1.2690 μm, (see Figures 13, 14 and Table 8).

B11 found isolated NH_3 features at 1.2340 μm and 1.2430 μm in the FIRE spectrum of UGPS 0722. There are peaks in the NH_3 absorption cross-sections at these wavelengths, corresponding to absorption features in our spectrum of UGPS 0722. There are no well-defined differences in the synthetic spectra with and without NH_3 opacity at these wavelengths. It may be that there are ammonia features at 1.2340 μm and 1.2430 μm which the model spectra are unable to identify. At the moment, these features are unconfirmed. B11 identified an NH_3+H_2O feature at 1.2367 μm. We find that this feature is an H_2O+NH_3 blend. B11 identified a feature at 1.2438 μm as an H_2O+CH_4 blend. There is a peak in the NH_3 opacity at this wavelength, corresponding to an absorption feature in our spectrum of UGPS 0722. However, the S12 synthetic spectra show no absorption feature at this location. We note that a synthetic spectrum naturally accounts for a range of temperatures in the line formation due to optical depth effects in and out of lines. This will affect lines that are particularly temperature sensitive and result in synthetic spectra that differ somewhat from opacity plots, even over a narrow range of wavelengths. While we believe this feature is most likely an NH_3 feature,

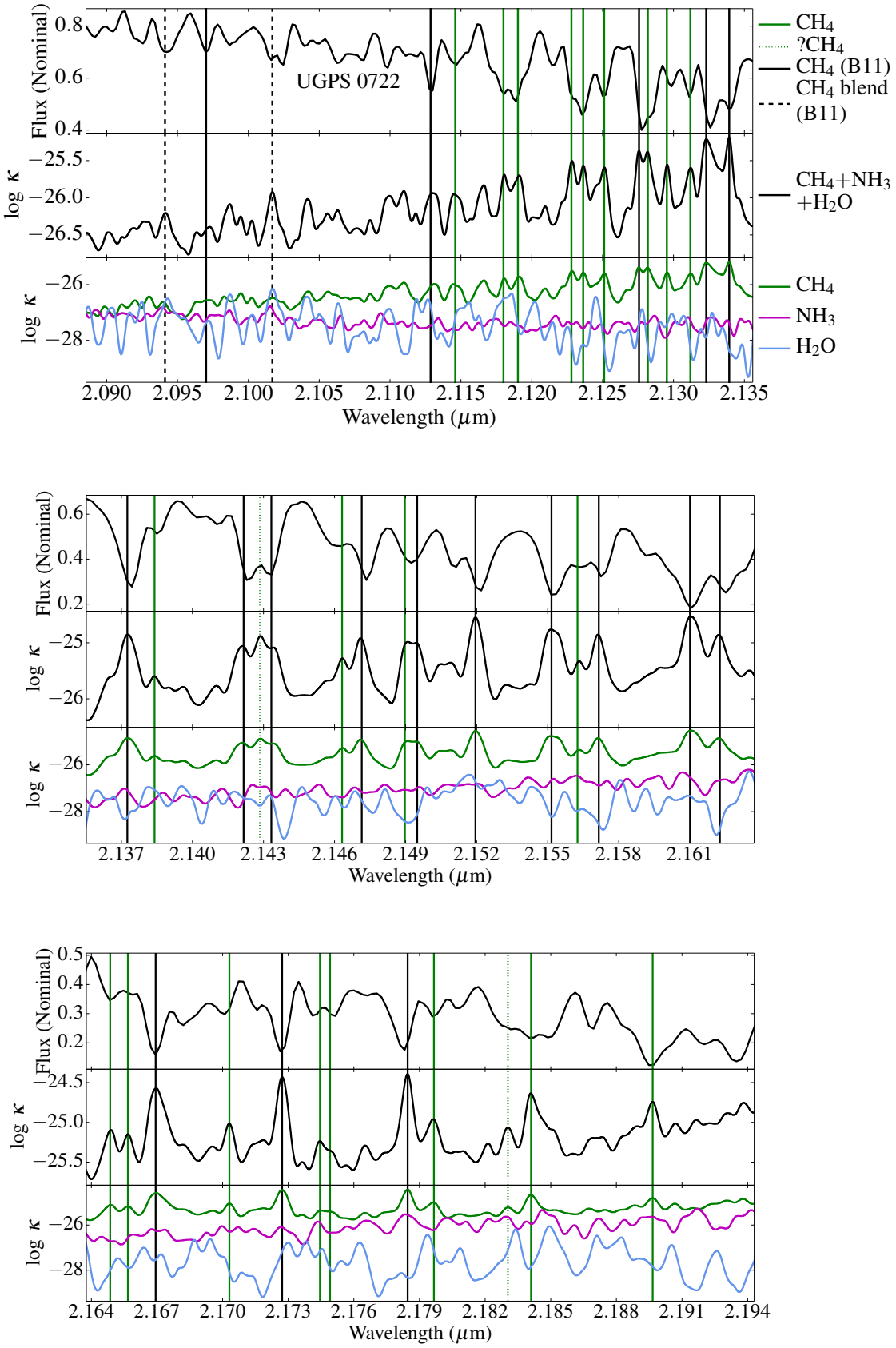

Figure 11. CH_4 absorption features in the K-band spectrum of UGPS 0722 (see Table 7). Solid black lines are features previously detected by B11. Solid green lines are features identified in this work. Black dashed lines are features identified by B11 as CH_4 features which we find to be due to CH_4 and one or more other molecular species.

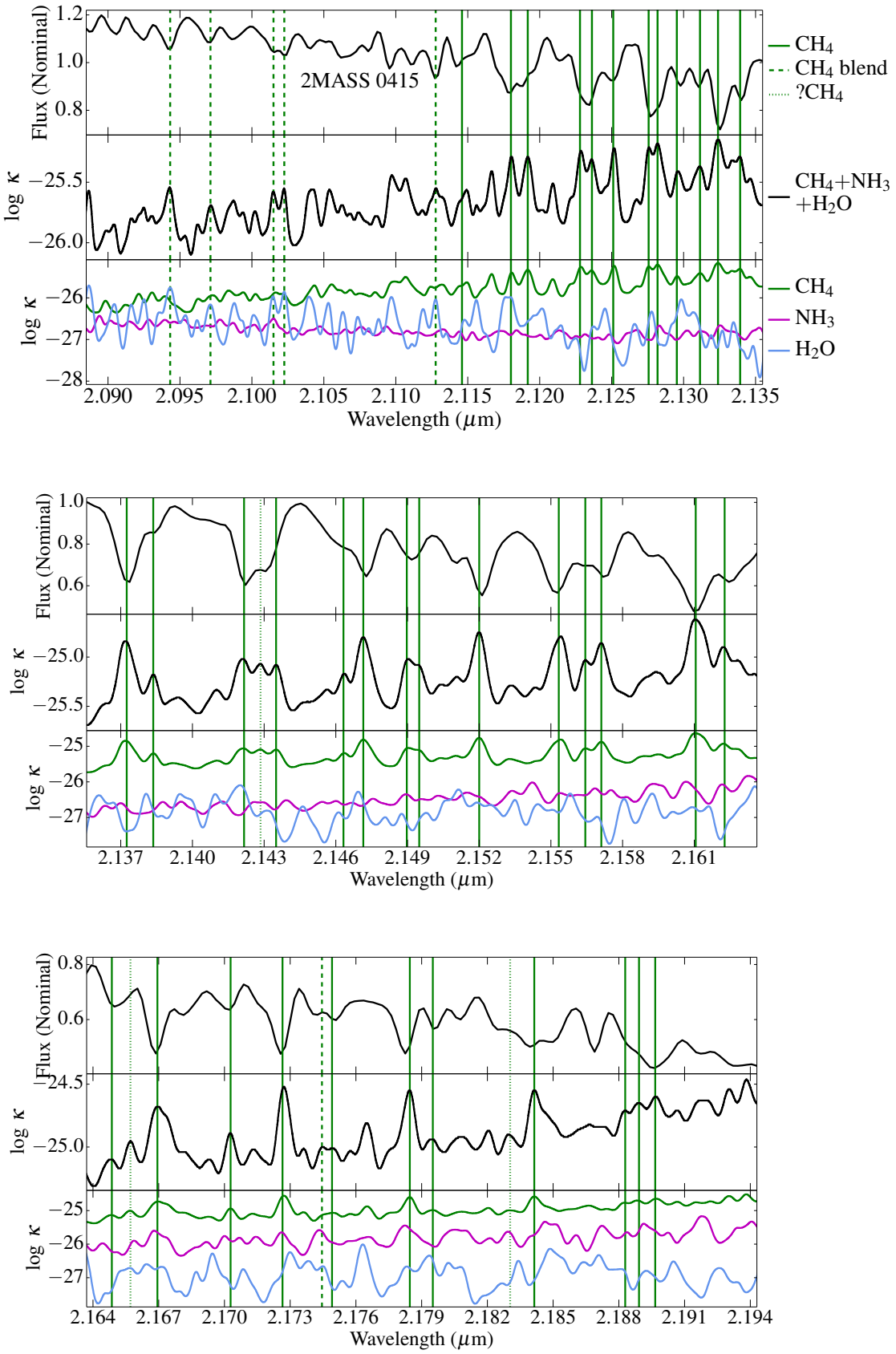

Figure 12. CH_4 features in the K-band spectrum of 2MASS 0415 (see Table 7).

Table 7. CH_4 Absorption Features in the K Band Spectra of Late T Dwarfs (see Figures 11 and 12)

Source	λ (μm)	Opacity Source (B11)	Opacity Source (500 K/750 K)	Absorption feature in UGPS 0722	Absorption feature in 2MASS 0415
B11	2.0943	CH_4	$(CH_4+H_2O+NH_3)/(H_2O+CH_4)$	Yes	Yes
B11	2.0971	CH_4	$CH_4/(CH_4+H_2O)$	Yes	Yes
B11	2.1017†	CH_4	$(CH_4+H_2O+NH_3)/(H_2O+CH_4)$	Yes	Yes
B11	2.1129	CH_4	$CH_4/(CH_4+H_2O)$	Yes	Yes
This work	2.1146	—	CH_4/CH_4	Yes	Yes
This work	2.1180	—	CH_4/CH_4	Yes	Yes
This work	2.1190	—	CH_4/CH_4	Yes	Yes
This work	2.1228	—	CH_4/CH_4	Yes	Yes
This work	2.1236	—	CH_4/CH_4	Yes	Yes
This work	2.1251	—	CH_4/CH_4	Yes	Yes
B11	2.1276	CH_4	CH_4/CH_4	Yes	Yes
This work	2.1282	—	CH_4/CH_4	Yes	Yes
This work	2.1295	—	CH_4/CH_4	Yes	Yes
This work	2.1312	—	CH_4/CH_4	Yes	Yes
B11	2.1323	CH_4	CH_4/CH_4	Yes	Yes
B11	2.1339	CH_4	CH_4/CH_4	Yes	Yes
B11	2.1373	CH_4	CH_4/CH_4	Yes	Yes
This work	2.1384	—	CH_4/CH_4	Yes	Yes(?)
B11	2.1421	CH_4	CH_4/CH_4	Yes	Yes
This work	2.1429	—	CH_4/CH_4	Yes(?)	Yes(?)
B11	2.1433	CH_4	CH_4/CH_4	Yes	Yes
This work	2.1463	—	CH_4/CH_4	Yes	Yes
B11	2.1472	CH_4	CH_4/CH_4	Yes	Yes
This work	2.1490	—	CH_4/CH_4	Yes	Yes
B11	2.1495	CH_4	CH_4/CH_4	Yes	Yes
B11	2.1520	CH_4	CH_4/CH_4	Yes	Yes
B11	2.1552	CH_4	CH_4/CH_4	Yes	Yes
This work	2.1564	—	CH_4/CH_4	Yes	Yes
B11	2.1572	CH_4	CH_4/CH_4	Yes	Yes
B11	2.1610	CH_4	CH_4/CH_4	Yes	Yes
B11	2.1623	CH_4	CH_4/CH_4	Yes	Yes
This work	2.1649	—	CH_4/CH_4	Yes	Yes
This work	2.1656	—	CH_4/CH_4	Yes	Yes(?)
B11	2.1669	CH_4	CH_4/CH_4	Yes	Yes
This work	2.1703	—	CH_4/CH_4	Yes	Yes
B11	2.1727	CH_4	CH_4/CH_4	Yes	Yes
This work	2.1745	—	$CH_4/(CH_4+NH_3)$	Yes	Yes
This work	2.1749	—	CH_4/CH_4	Yes	Yes
B11	2.1784	CH_4	CH_4/CH_4	Yes	Yes
This work	2.1797	—	CH_4/CH_4	Yes	Yes
This work	2.1830	—	CH_4/CH_4	Yes(?)	No
This work	2.1841	—	CH_4/CH_4	Yes	Yes
This work	2.1897‡	—	CH_4/CH_4	Yes	Yes

† In 2MASS 0415, two adjacent peaks in H_2O/CH_4 opacity coincide with absorption features at 2.1015 μm and 2.1023 μm.
‡ In 2MASS 0415, this feature corresponds to three adjacent peaks in CH_4 opacity at 2.1883 μm, 2.1889 μm and 2.1897 μm.

it remains unconfirmed. In general, higher resolution spectroscopy will greatly assist the identification of lines and absorbers.

While the peak in the NH_3 opacity at 1.2540 μm does not appear strong enough to account for the depth of the corresponding absorption feature in the spectrum of UGPS 0722, there is a change in slope at this wavelength between the synthetic spectra with and without NH_3 opacity, suggesting that ammonia opacity does make a contribution to this feature.

The ro-vibrational transitions responsible for the NH_3 absorption features in the J-band spectra of the two T dwarfs are P-branch transitions, with the exception of a relatively weak Q-branch transition line in the feature at 1.2284 μm, and a relatively strong R-branch transition line in the feature at 1.2494 μm. Contrast this with the ro-vibrational transition lines responsible for the CH_4 absorption features in the J-band, which are all R-branch transition lines. Here, the shorter wavelength P-branch transitions arise from the $\nu_1+3\nu_4$ vibrational band, while the longer wavelength P-branch transition lines, and the single Q-branch transition line, are from the $\nu_1+\nu_3+\nu_4$ vibrational band. The single R-branch transition line is from the $\nu_2+2\nu_3$ vibrational band.

4.3 The H-Band

Figure 5 in C11 shows that NH_3 is the dominant source of opacity across the blue wing of the H-band (1.50-1.59 μm) in T dwarfs with $T_{eff} \leqslant 600$ K. We also find that this is

Table 8. Absorption features and spectroscopic signatures of NH_3 in the J band spectra of late T dwarfs (see Figures 13 and 14)

Source	λ (μm)	Opacity Source (500 K/750 K)	NH_3 feature in synthetic spectrum (500 K/750 K)	Feature in UGPS 0722	Feature in 2MASS 0415
This work	1.2249	NH_3/(H_2O+NH_3)	Yes/No	Yes	Yes
This work	1.2265	NH_3/(NH_3+CH_4+H_2O)	Yes/No	Yes(?)	Yes(?)
This work	1.2284§	NH_3/—	Yes/No	Yes(?)	Yes
This work	1.2300	(H_2O+NH_3)/NH_3	Yes/Yes	Yes(?)	No
This work	1.2326§	(NH_3+H_2O)/H_2O	No(?)/No	Yes	Yes
B11	1.2340	NH_3/(NH_3+H_2O)	No(?)/No	Yes	Yes(?)
This work	1.2355	NH_3/(NH_3+CH_4)	Yes/Yes	Yes	Yes(?)
B11	1.2367	(H_2O+NH_3)/H_2O	No/No	Yes	Yes
This work	1.2378†	NH_3/NH_3	Yes/No	Yes	Yes
This work	1.2394††	NH_3/NH_3	Yes/Yes	No	Yes
This work	1.2406	NH_3/H_2O	Yes/No	Yes	Yes
B11	1.2430§	NH_3/—	No(?)/No	Yes	No
B11	1.2438§	NH_3/—	No(?)/No	Yes	No
This work	1.2494	NH_3/NH_3	Yes/Yes(?)	No	Yes(?)
This work	1.2535§	NH_3/—	No(?)/No	Yes	No
B11	1.2540	(NH_3+CH_4)/(H_2O+NH_3)	Yes/No	Yes	Yes
This work	1.2578§	NH_3/—	Yes(?)/No	No	Yes
This work	1.2624	NH_3/H_2O	No/No	Yes	Yes
This work	1.2635‡	NH_3/H_2O	No/No	Yes	Yes
B11	1.2661§	(NH_3+CH_4)/—	No/No	Yes	Yes

§ There is no obvious opacity source corresponding to an absorption feature at this wavelength in the spectrum of 2MASS 0415.
† In 2MASS 0415, the peak in NH_3 opacity is at 1.2381 μm.
†† In 2MASS 0415, this feature corresponds to two adjacent peaks in NH_3 opacity at 1.2394 μm, and 1.2399 μm.
‡ In 2MASS 0415, the peak in NH_3 opacity is at 1.2638 μm.
In tables 8, 9, and 10, ammonia features produced by R-, Q-, and P-branch line transitions are highlighted in red, grey, and blue respectively.

the case. In contrast, CH_4 is by two orders of magnitude the dominant opacity source on the red slope of the H-band peak flux. At 750 K, the NH_3 and H_2O scaled absorption cross-sections are of the same order of magnitude. Therefore, some features that are produced by NH_3 only in the spectrum of UGPS 0722, are produced by a combination of ammonia and water opacities in the spectrum of 2MASS 0415. These results are summarised in Figures 15, 16 and Table 9.

B11 observed a number of "pure" NH_3 absorption features. Of these, the feature at 1.5140 μm corresponds to a peak in both NH_3 and H_2O opacity. The strengths of the opacities are broadly similar. There is no significant difference in the model spectra computed with and without NH_3 opacity, other than a small change in amplitude. Therefore, we conclude that this feature is most likely an ammonia/water blend. The feature at 1.5152 μm corresponds to a peak in NH_3 opacity and absorption features in UGPS 0722 and 2MASS 0415. There appears to be a difference in opacity between the model spectrum computed at 500 K but not that computed at 750 K, other than in amplitude. We confirm that this NH_3 absorption feature is due entirely to NH_3 in the spectrum of UGPS 0722, but is an NH_3+H_2O feature in 2MASS 0415. The feature at 1.5282 μm corresponds to a peak in NH_3 opacity and to a clear difference between the S12 model spectra computed at 500 K. The model spectra show that without NH_3 opacity a rather strong peak would be expected at 1.5282 μm while only a small one is present. Indeed, the spectrum of UGPS 0722 does look similar to the model spectrum with NH_3 opacity. The spectrum of 2MASS 0415 at this wavelength looks similar to UGPS 0722, suggesting that NH_3 opacity is again the dominant opacity source. However, the synthetic spectra computed at 750 K show two relatively strong peaks, which differ only in amplitude between the two spectra. The scaled molecular opacities at 750 K suggest that the feature in 2MASS 0415's spectrum is produced by a blend of H_2O+NH_3 opacity and we have listed this as such in Table 9.

In addition, we believe we have identified eight new NH_3 absorption features that correspond both to peaks in the NH_3 opacity and differences between the model spectra with and without NH_3. Among these, the feature at 1.5240 μm corresponds to peaks in the NH_3 opacity at 500 K and 750 K. While there is no obvious minimum in the spectrum of UGPS 0722 at this wavelength, the shape of the spectrum is most similar to the synthetic spectrum with NH_3 opacity at 500 K. This is an instance where we have identified an absorption feature based on the similarity of the shape of a T dwarf's spectrum to the shape of a synthetic spectrum, rather than the correspondence of a peak in molecular opacity with a trough in the T dwarf's flux. The spectrum of 2MASS 0415 at this wavelength looks most similar to the synthetic spectrum without NH_3 opacity at 750 K. The feature at 1.5327 μm also corresponds to peaks in the NH_3 opacity at 500 K and 750 K and there appear to be absorption features at this wavelength in both T dwarf spectra. We note that at this wavelength there is a "shoulder" in the synthetic spectrum without NH_3 opacity at 500 K which is missing in the synthetic spectrum with NH_3 opacity. This feature is present in the synthetic spectra with and without NH_3 opacity calculated at 750 K. Finally, the S12 models at 500 K predict a feature at 1.5382 μm. This feature is missing in the spectra of both T dwarfs.

Table 9. Absorption features and spectroscopic signatures of NH_3 in the H band spectra of late T dwarfs (see Figures 15 and 16)

Source	λ (μm)	Opacity Source (500 K/750 K)	NH_3 feature in synthetic spectrum (500 K/750 K)	Feature in UGPS 0722	Feature in 2MASS 0415
B11	1.4996	$(H_2O+NH_3)/(H_2O+NH_3)$	No/No	Yes	Yes
B11	1.5020	$(NH_3+H_2O)/H_2O$	No/No	Yes	Yes
B11	1.5086	NH_3/H_2O	No/No	Yes	Yes
B11	1.5140	$(NH_3+H_2O)/(NH_3+H_2O)$	No/No	Yes	Yes
B11	1.5152	$NH_3/(H_2O+NH_3)$	Yes/No	Yes	Yes
B11	1.5179§	NH_3/—	Yes/No	Yes	Yes
B11	1.5201	$NH_3/(NH_3+H_2O)$	Yes/Yes	Yes	Yes
This work	1.5224	$NH_3/(NH_3+H_2O)$	Yes/No	Yes	Yes
This work	1.5240	$NH_3/(NH_3+H_2O)$	Yes/No(?)	Yes	Yes(?)
B11	1.5260	$NH_3/(NH_3+H_2O)$	Yes(?)/No	No(?)	Yes
B11	1.5270	$NH_3/(H_2O+NH_3)$	Yes(?)/No	Yes	Yes
B11	1.5282	$NH_3/(H_2O+NH_3)$	Yes/No	Yes	Yes
This work	1.5297	$NH_3/(H_2O+NH_3)$	Yes(?)/No	Yes	Yes
B11	1.5305	$(NH_3+H_2O)/(H_2O+NH_3)$(?)	Yes(?)/No	Yes	Yes
B11	1.5327	$NH_3/(NH_3+H_2O)$	Yes/No	Yes	Yes
B11	1.5352	$(NH_3+H_2O)/(H_2O+NH_3)$	Yes(?)/No	Yes	Yes
This work	1.5367	$NH_3/(NH_3+H_2O)$	Yes/No	Yes	Yes
This work	1.5382†	NH_3/NH_3	Yes/Yes(?)	No	No
This work	1.5395§	NH_3/—	Yes/No	Yes	Yes(?)
B11	1.5408	$NH_3/(NH_3+H_2O)$	Yes(?)/No	Yes	Yes
This work	1.5427 ††	$NH_3/(H_2O+NH_3)$	Yes/No	Yes	Yes
B11	1.5440	NH_3/H_2O	Yes(?)/No	Yes	Yes
B11	1.5480‡	$NH_3/(H_2O+NH_3)$	Yes(?)/No	Yes	Yes
B11	1.5504§	NH_3/—	Yes/No	Yes	Yes
This work	1.5533	NH_3/NH_3	Yes/Yes	No	No
This work	1.5545	NH_3/NH_3	Yes/No	Yes	Yes
B11	1.5609§	$(NH_3+CH_4+H_2O)$/ —	No/No	Yes	Yes
B11	1.5660	$NH_3/(NH_3+H_2O)$	Yes/No	Yes	Yes
B11	1.5687	$NH_3/(NH_3+H_2O)$	No/No	Yes	Yes
B11	1.5735	NH_3/NH_3	Yes/No	Yes	Yes
B11	1.5805‡‡	$(NH_3+H_2O)/(NH_3+H_2O)$	No/No	Yes	Yes
B11	1.5897§	(NH_3+CH_4)/—	No/No	No(?)	No(?)
B11	1.5905§	$(NH_3+CH_4+H_2O)$/—	No/No	No(?)	No(?)

§ The absorption feature in 2MASS 0415 does not correspond to a peak in any of the opacity sources considered here.
† In 2MASS 0415, the peak in NH_3 opacity is at 1.5386 μm.
†† In 2MASS 0415, the peak in NH_3 opacity is at 1.5425 μm.
‡ In 2MASS 0415, the absorption feature due to H_2O+NH_3 opacity is centred at ∼1.5477 μm.
‡‡ In 2MASS 0415, the peak in NH_3 opacity is at 1.5803 μm.

We have found no significant differences in the identities of the ro-vibrational lines responsible for the absorption features in the two T dwarfs. The two blended NH_3 features at the shortest wavelengths, 1.4996 μm and 1.5020 μm, are produced by R-branch line transitions. A weak Q-branch transition line is found in the feature at 1.4996 μm. The R-branch transition lines belong to the $\nu_1+\nu_3$ vibrational band, while the single Q-branch line arises from the the $\nu_1+2\nu_4$ band.

NH_3 features in the H-band are produced by ro-vibrational transitions from the P-, Q-, and R-branches. Compare this with the CH_4 absorption features in the H-band which are also produced by ro-vibrational transitions from all three branches. However, most of the NH_3 absorption features in the H-band are produced by P-branch transition lines, while the CH_4 absorption features in the H-band are almost equally distributed across the P-, Q-, and R-branches. Q-branch transition lines are mostly from the $\nu_1+\nu_3$ vibrational band. However, of the four strongest transition lines responsible for the absorption feature at 1.5152 μm, while three lines are Q-branch transition lines, two of these lines include overtones. These two lines have approximately half the intensity of the Q-branch line from the $\nu_1+\nu_3$ vibrational band. Another line responsible for the feature at 1.5152 μm is a P-branch transition line from the $2\nu_2+3\nu_4$ vibrational band. This line has approximately twice the intensity of the strongest Q-branch line. The absorption features at 1.5179 μm and 1.5201 μm also contain single P-branch transition lines with overtones. The feature at 1.5201 μm also contains a Q-branch transition line with an overtone. As expected, this line is approximately half the strength of the other Q-branch transition lines. In the absorption features produced by P-branch line transitions (1.5224-1.5905 μm), there are a few Q-branch transition lines in the absorption features at longer wavelengths. Otherwise, absorption features are entirely due to P-branch transition lines. However, these lines belong to a larger assortment of vibrational bands than is the case for absorption features due to R- or Q-branch transition lines. Approximately half the absorption features are produced by transition lines belonging to the $\nu_1+\nu_3$ vibrational band, while

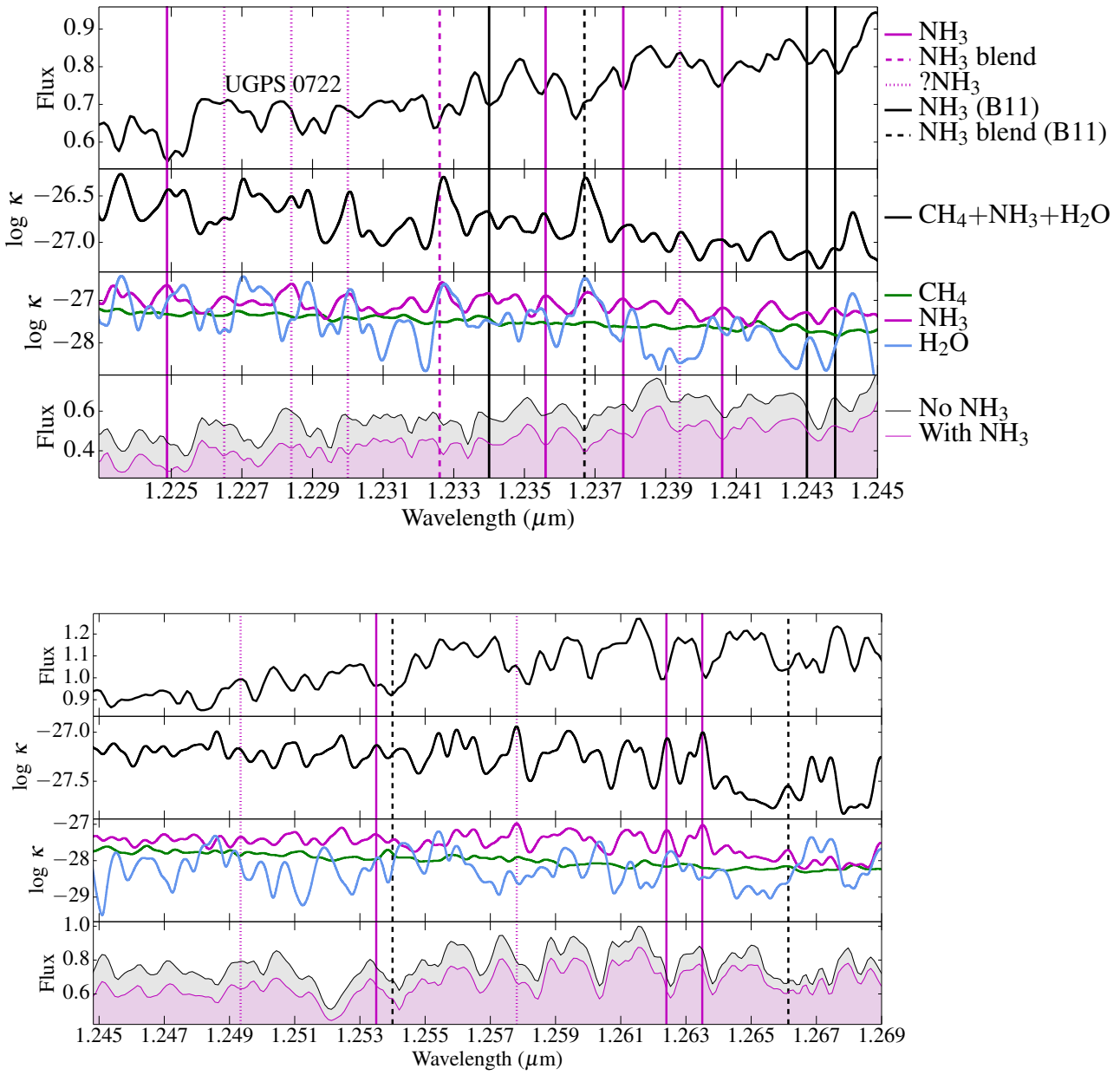

Figure 13. NH_3 absorption in the J-band spectrum of UGPS 0722 (see Table 8). Absorption cross-sections, scaled for molecular abundances, are calculated at 500 K for CH_4 (green), H_2O (blue) and NH_3 (magenta). The lowest graph contains S12 synthetic spectra with NH_3 opacity (magenta shade) and without NH_3 opacity (grey shade), also calculated at 500 K. Solid magenta lines are NH_3 features identified in this work. The dashed magenta line is an NH_3/H_2O feature identified in this work. Dotted magenta lines are features which are predicted by the scaled opacity cross-section and the S12 models but which are either missing or ambiguous. Solid and dashed black lines indicate features identified by B11.

somewhat less than half the features are from the $\nu_1+2\nu_4$ vibrational band. It does appear that absorption features at shorter wavelengths belong predominantly to the $\nu_1+\nu_3$ vibrational band, while those at longer wavelengths arise from the $\nu_1+2\nu_4$ vibrational band. One of the strongest transition lines producing the NH_3 absorption feature at the longest wavelength, 1.5905 μm, is the $4\nu_4$ overtone. These results are described in more detail in the online tables A1-A5 and B1-B6.

4.4 The K-Band

In the K-band, S12 identified 19 absorption features corresponding to peaks in NH_3 opacity. Eight of these features matched absorption features in the Magellan/FIRE spectrum of UGPS 0722. A further six absorption features were tentatively identified. The remaining five features did not have any counterparts in the T dwarf spectrum.

We have been able to confirm the eight absorption

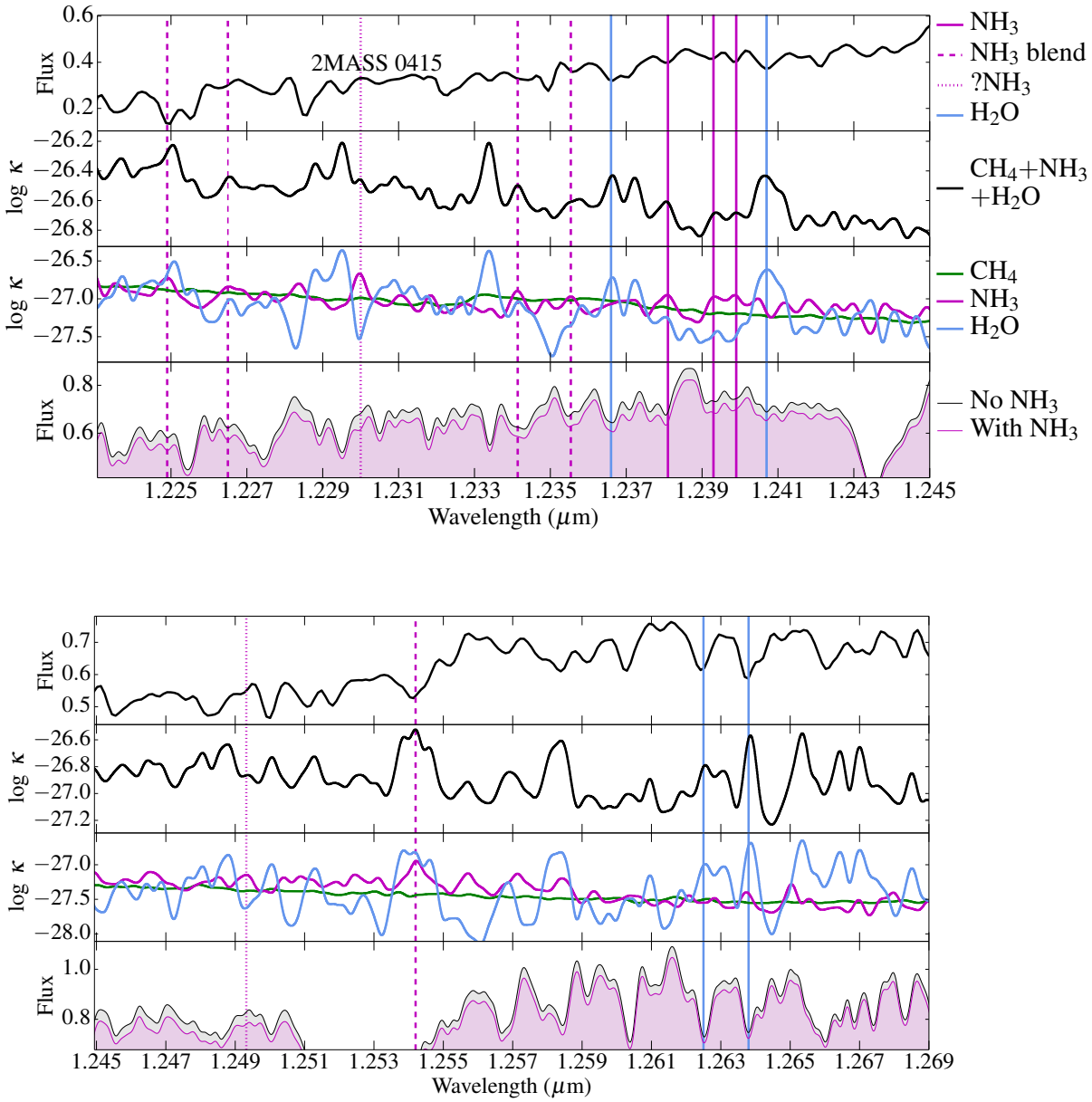

Figure 14. NH_3 absorption features in the *J*-band spectrum of 2MASS 0415 (see Table 8). Features are as described in the *J*-band spectrum of UGPS 0722. The solid blue lines are pure H_2O features which were NH_3+H_2O blends in the spectrum of UGPS 0722. The deep absorption features centred at ∼1.243 μm and ∼1.253 μm in the synthetic spectra, are the blue and red components of the K I doublet.

features first identified by S12. We are also able to confirm seven of the uncertain/missing detections, one of which appears to be an NH_3+H_2O blend. In addition, we have identified six new absorption features, including another NH_3+H_2O blend. There is a notch in the spectrum of UGPS 0722 at 1.9937 μm corresponding to where NH_3 opacity removes a large peak in the synthetic spectrum without NH_3 opacity. While there is no peak in NH_3 opacity at this wavelength, adding NH_3 removes a trough in the total opacity that would otherwise exist. We interpret this as an NH_3 signature. In 2MASS 0415, the observed spectrum is also a better fit to the 750 K model spectrum with NH_3 opacity than without NH_3 opacity. In this case, ammonia opacity covers a gap in water opacity and removes a spike in the 750 K model spectrum. These results are summarised in Figures 17, 18, and Table 10.

The absorption feature identified by B11 at 1.9900 μm as due to a combination of ammonia and water opacity does not correspond to a change in ammonia opacity in the S12 models. However, Figure 17 suggests that water opacity rather than ammonia opacity is the stronger component in this feature. Indeed, in the spectrum of 2MASS 0415 the water opacity at this wavelength is an order of magnitude stronger.

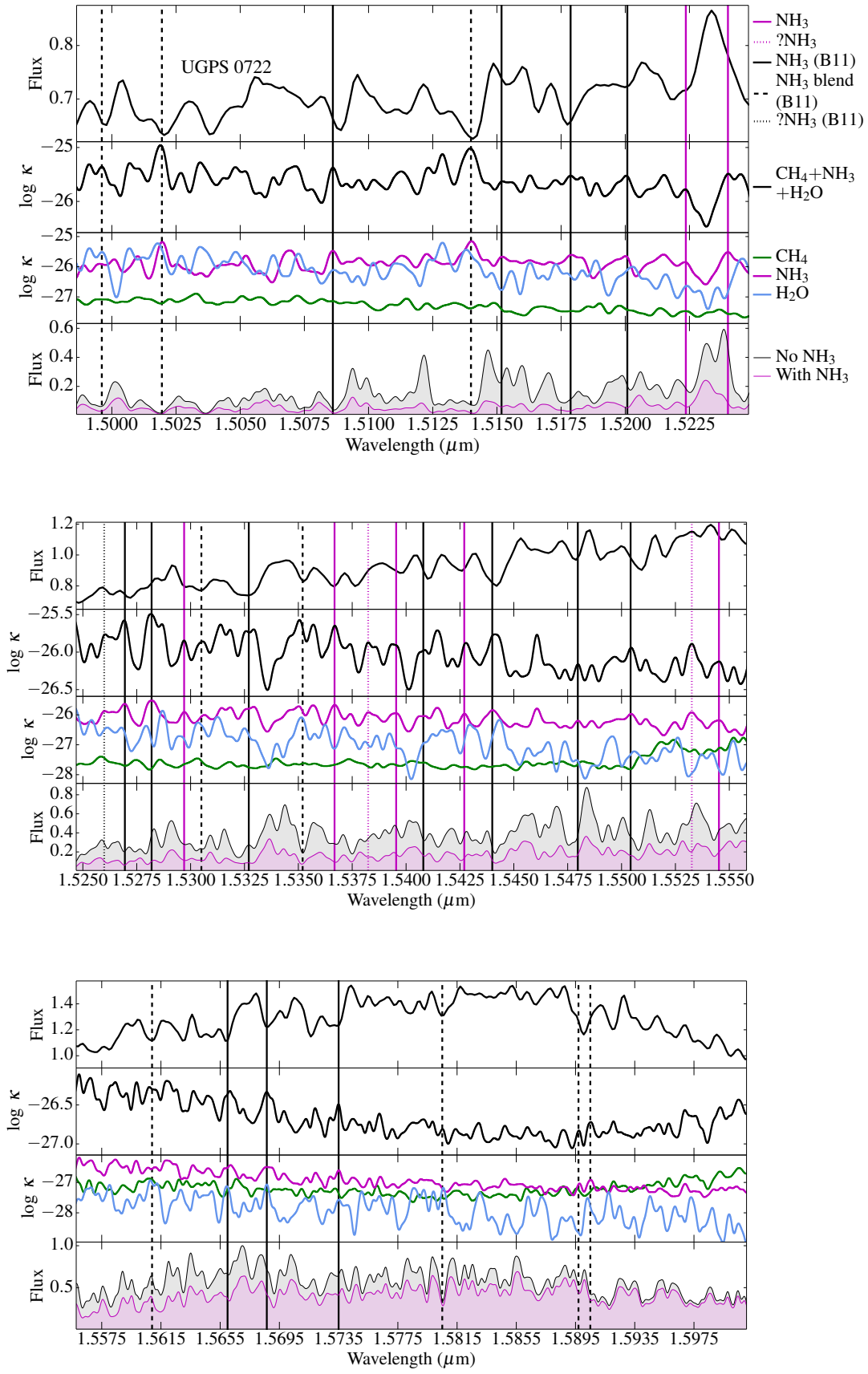

Figure 15. NH_3 absorption features in the H-band spectrum of UGPS 0722 (see Table 9). Scaled absorption cross-sections are calculated at 500 K for CH_4 (green), H_2O (blue) and NH_3 (magenta). Features are as described in Figure 13. Dashed lines are features produced by a combination of molecular species. The dotted lines are NH_3 features predicted by the S12 models, but missing or ambiguous in the data.

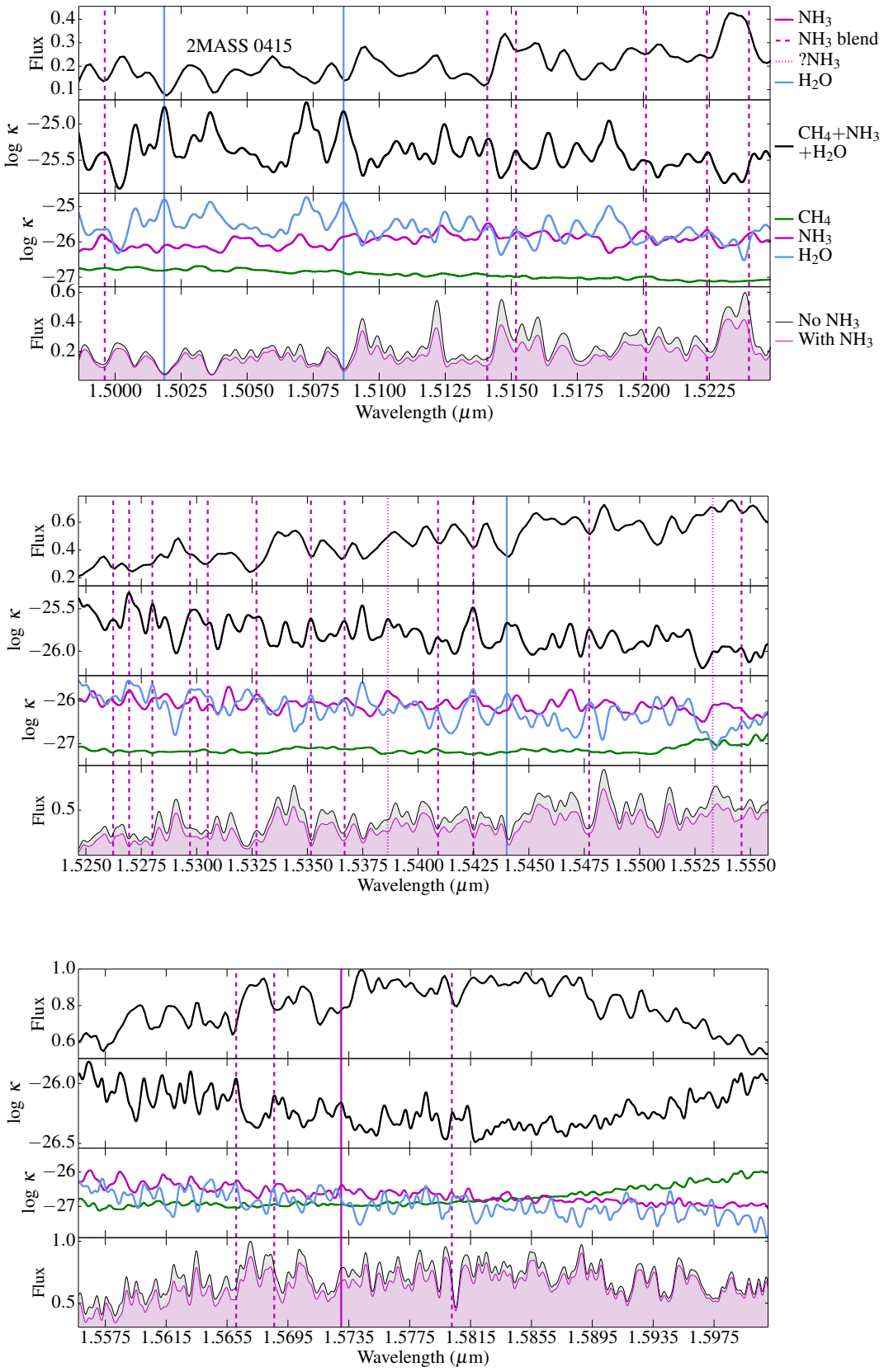

Figure 16. Opacity sources responsible for the corresponding absorption features in the *H*-band spectrum of 2MASS 0415 (see Table 9). Features are as described in Figures 13 and 15. Scaled absorption cross-sections are calculated at 750 K for CH_4 (green), H_2O (blue) and NH_3 (magenta).

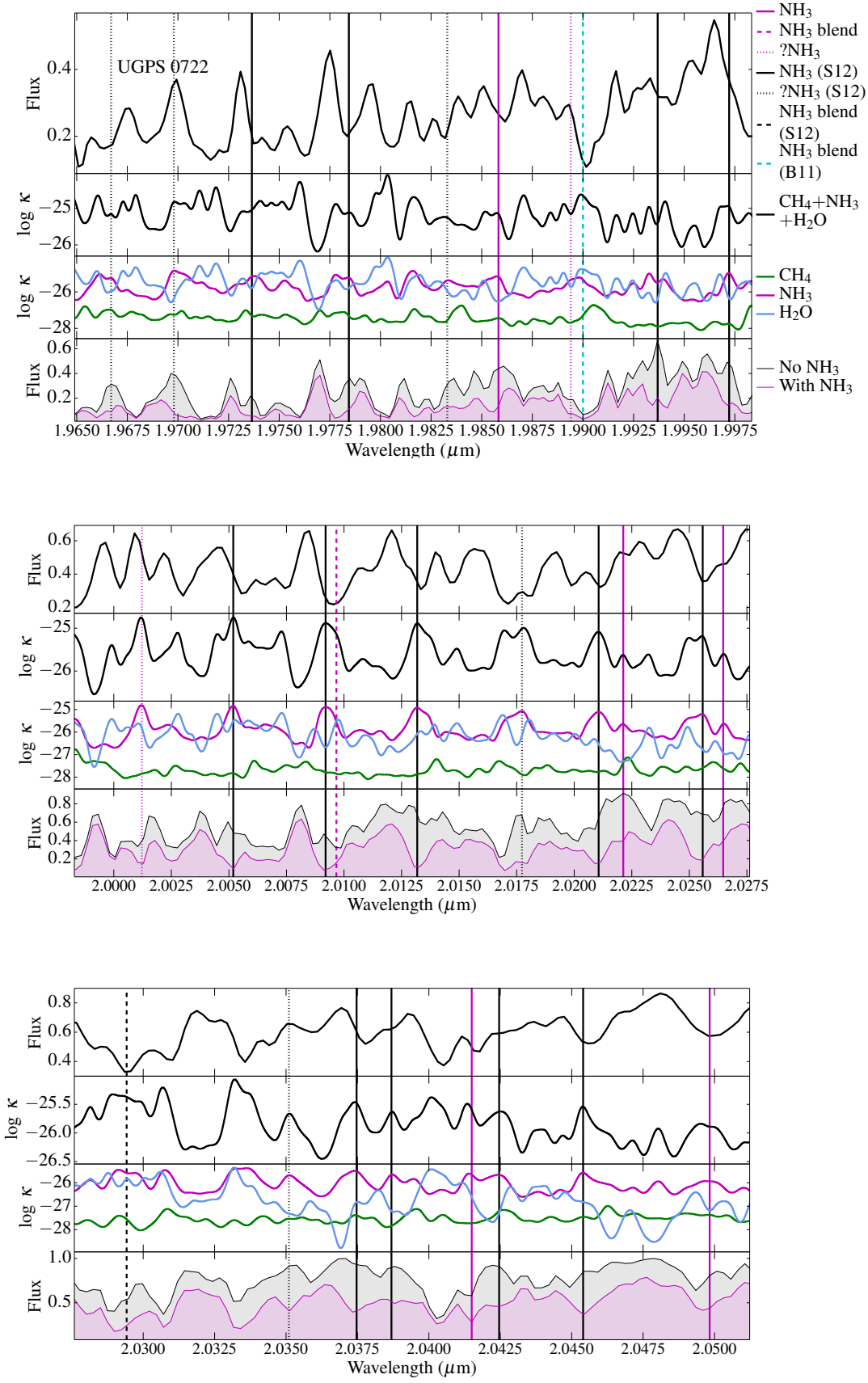

Figure 17. NH_3 absorption features in the K-band spectrum of UGPS 0722 (see Table 10). Solid black lines are features in S12 which we can now confirm. These include seven features which were either missing or ambiguous in S12. The black dotted lines are four S12 features which remain missing. The solid magenta lines are features detected in this work. Scaled absorption cross-sections are calculated at 500 K for CH_4 (green), H_2O (blue) and NH_3 (magenta).

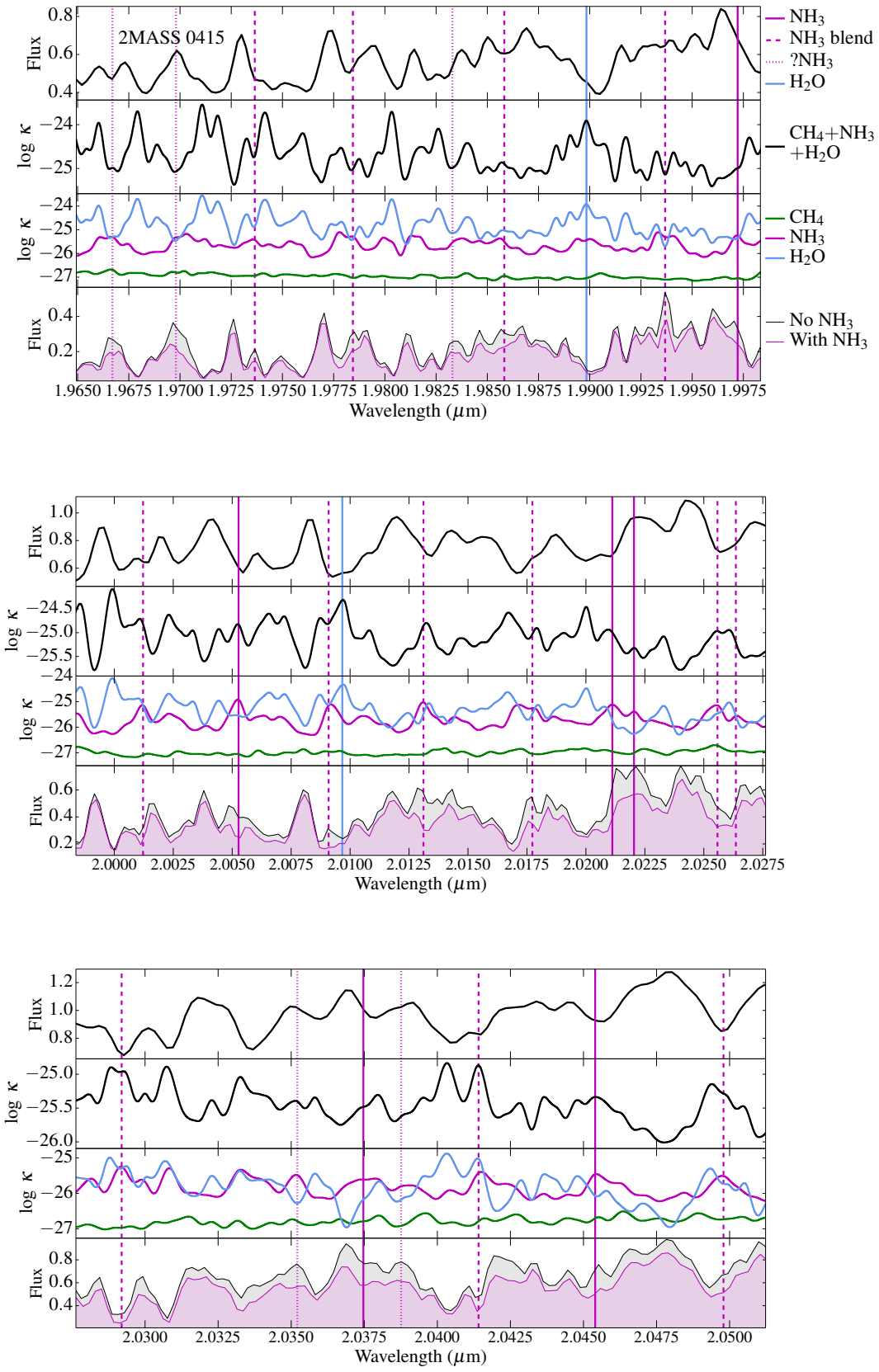

Figure 18. NH_3 absorption features in the K-band spectrum of 2MASS 0415 (see Table 10). Scaled absorption cross-sections are calculated at 750 K for CH_4 (green), H_2O (blue) and NH_3 (magenta).

Table 10. Absorption features and spectroscopic signatures of NH_3 in the K band spectra of late T dwarfs (see Figures 17 and 18)

Source	λ (μm)	Opacity Source (500 K/750 K)	NH_3 feature in synthetic spectrum (500 K/750 K)	Feature in UGPS 0722	Feature in 2MASS 0415
S12	1.9667	NH_3/(NH_3+H_2O)	Yes/Yes	No(?)	No(?)
S12	1.9698	NH_3/NH_3	Yes/Yes	No	No
S12	1.9737	NH_3/(H_2O+NH_3)	Yes/No	Yes	Yes(?)
S12	1.9784	(NH_3+H_2O)/(NH_3+H_2O)	Yes/Yes	Yes	Yes(?)
S12	1.9833	(NH_3+H_2O)/(H_2O+NH_3)	Yes/Yes(?)	Yes(?)	No
This work	1.9858	NH_3/(H_2O+NH_3)	Yes/Yes	Yes	Yes
This work	1.9894[§]	NH_3/—	Yes/Yes(?)	No	Yes(?)
B11	1.9900[†]	(H_2O+NH_3)/H_2O	No/No	Yes	Yes
S12	1.9937	NH_3/(H_2O+NH_3)	Yes/Yes	Yes	Yes(?)
S12	1.9972	NH_3/NH_3	Yes/Yes	Yes	Yes
This work	2.0012	NH_3/(H_2O+NH_3)	Yes/No	No	Yes
S12	2.0052	NH_3/NH_3	Yes/Yes	Yes	Yes
S12	2.0092	NH_3/(NH_3+H_2O)	Yes/Yes	Yes	Yes
This work	2.0097	(NH_3+H_2O)/H_2O	Yes/No	Yes	Yes
S12	2.0132	NH_3/(NH_3+H_2O)	Yes/Yes	Yes	Yes
S12	2.0177	NH_3/(NH_3+H_2O)	Yes/Yes	No(?)	Yes
S12	2.0211	NH_3/NH_3	Yes/Yes	Yes	Yes
This work	2.0221	NH_3/NH_3	Yes/Yes	Yes	Yes
S12	2.0256	NH_3/(NH_3+H_2O)	Yes/Yes	Yes	Yes
This work	2.0265	NH_3/(NH_3+H_2O)	Yes/No	Yes	Yes
S12	2.0294	(NH_3+H_2O)/(H_2O+NH_3)	Yes/No	Yes	Yes
S12	2.0351	NH_3/NH_3	Yes/Yes	No	No
S12	2.0375	NH_3/NH_3	Yes/No(?)	Yes	Yes
S12	2.0387	NH_3/(NH_3+H_2O)	Yes/Yes	Yes	No
This work	2.0415	NH_3/(H_2O+NH_3)	Yes/No(?)	Yes	No(?)
S12	2.0425[§]	NH_3/—	Yes/Yes	Yes	Yes
S12	2.0454	NH_3/NH_3	Yes/Yes	Yes	Yes
This work	2.0498	NH_3/(NH_3+H_2O)	Yes/Yes(?)	Yes	Yes

[§] The absorption feature in 2MASS 0415 does not correspond to a peak in any of the opacity sources considered here.
[†] In 2MASS 0415, the peak in H_2O opacity is at 1.9898 μm.

In the ro-vibrational spectrum for this region of the K-band, there is a weak $4\nu_2$ overtone among the transition lines contributing to the absorption feature at 2.0132 μm. Otherwise all the NH_3 absorption features in the K-band belong to the ν_1+ν_4 vibrational band. Approximately 71% of the absorption features are produced by P-branch transition lines. There is a single feature at 1.9667 μm produced by R-branch transitions alone, and there is a very strong R-branch transition line among the Q-branch transition lines responsible for the absorption feature at 1.9737 μm. The remaining ∼25% absorption features are generated by Q-branch transitions. Note that NH_3 absorption features in the K-band spectra of these two T dwarfs are produced by transition lines from the P-, Q-, and R-branches, whereas we found only R-branch transition lines in the K-band absorption features due to CH_4.

5 DISCUSSION

In our analysis of CH_4 absorption features, we have assumed that the spectra of each T dwarf can be interpreted using an opacity spectrum computed at a single temperature. Absorption features tend to be produced in the higher, cooler parts of the photosphere. While it is possible that an absorption feature seen in the spectrum of 2MASS 0415 may be better modelled with a 500 K opacity spectrum than a 750 K opacity spectrum, we have not found any examples of this. This gives us confidence in the accuracy of the line lists and model spectra we have used in our analysis. We have determined that the strongest absorption features on the long side of the H- and K-band flux peaks of both T dwarfs are due to CH_4 opacity (apart from mixed absorption features at 2.0943 μm and 2.1017 μm in the spectra of both T dwarfs, and mixed features at 2.0971 μm, and 2.1129 μm in the spectrum of 2MASS 0415). There are significant differences between opacity sources in the spectra of the two T dwarfs on the long side of the J-band flux peak, where we identified a single methane feature in the spectrum of 2MASS 0415, compared to six features in the spectrum of UGPS 0722. There is a large number of methane blends in the J-band spectra of these objects compared to the pure methane features we have observed in these objects' H- and K-band spectra.

The disagreement between the 10to10 line list and the science data between 1.6145 μm-1.6258 μm (see Figures 8 and 9) cannot be due to faulty calibration of either the science spectra or the 10to10 line list, since elsewhere the correspondence between methane opacity and absorption feature is excellent. From our discussion in Section 3.4, it appears that the disparity is most probably due to a deficiency in the 10to10 line list in this wavelength region. The differences in wavelength are slight. This, together with the better agreement obtained with the hybrid list including experimental

data lead us to believe that the absorption features in the T dwarfs' spectra are due to methane.

The discrepancy between the 10to10 line list and the H-band data prompted us to ask whether some vibrational bands are more accurately represented in the 10to10 line list than others. To examine this, we looked at the vibrational band centres around 1.6 μm. The errors in the 10to10 line list were assessed by comparing the experimental data from HITRAN 2012 (Rothman et al. 2013). The errors are systematic within each vibrational band, reflecting the quality (or flaws) of the underlying potential energy surfaces (PES), which in the case of 10to10 was obtained by refining an ab initio PES to available experimental energies. We found that the band centres with the worst accuracy are for $\nu_1+2\nu_2$ and $\nu_3+2\nu_4$ where the accuracy is typically $\sim 8\times10^{-3}$ μm. These are probably the weakest band centres, especially the former where the intensity of the associated line transitions is of the order of two magnitudes weaker than those due to the $2\nu_3$ band. We have found that the band centre for $2\nu_3$ is the most accurate, with accuracies varying between $\sim 2\times10^{-6}$ μm and $\sim 8\times10^{-5}$ μm. All the methane features we have identified in the H-band are from this vibrational band. We looked at other line transitions involving one quantum of ν_3. These transitions are weaker than those from the $2\nu_3$ band and are comparable in strength to line transitions arising from vibrational bands other than $2\nu_3$ in this wavelength region. Our results are shown in Table 11.

While several ammonia absorption features predicted by the S12 model spectra between ∼1.223-1.235 μm remain undetected, we have found a number of others. Although the S12 model spectra with and without NH_3 opacity show no significant differences at the wavelengths corresponding to several possible NH_3 absorption features between ∼1.239-1.266 μm, we find that NH_3 opacity is the strongest opacity source in this region (see Figures 13 and 14). The failure of the S12 model spectra to predict these features may be because without a comprehensive, high-temperature methane line list, the models overestimate the importance of methane opacity in this region.

It has recently been suggested that the relatively red $J-H$ and $J-K$ colours seen in T dwarfs of spectral types $\gtrsim$T8 in comparison with model predictions could be explained by the formation of sulphide clouds [M12]. The model spectra used in the analyses here and in S12 are cloudless. While the BYTe line list and the improved calculations of H_2 CIA have reddened the $J-K$ colours of model spectra for T dwarfs with T_{eff} $\gtrsim$600 K, the reddening is insufficient to match the observed colours of the coolest T dwarfs [M12]. It is also possible that the inclusion of sulphide cloud opacity in a new set of synthetic spectra may be a better match to the data.

In UGPS 0722, NH_3 ro-vibrational transition lines in the H-band are an order of magnitude stronger than those in the J-band and NH_3 is the dominant source of opacity across the blue wing of the H-band (1.50-1.59 μm) (see Figure 15). This region of the H-band shows clear differences in the species responsible for the absorption features in the two T dwarfs' spectra. At 750 K, the scaled absorption cross-sections are of the same order of magnitude for all three of the main molecular opacity sources (H_2O, CH_4, NH_3) so that features due to NH_3 opacity alone in the spectrum of UGPS 0722, are produced by a combination of opacities in the spectrum of 2MASS 0415 (see Figure 16).

C11 detected absorption in the H-band spectrum of the Y dwarf WISEP J1738+2732 which corresponded to the $\nu_1+\nu_3$ absorption band of NH_3 but were unable to confirm this owing to the low resolution of their data. Our results confirm C11's findings. Indeed, the intensity of the ro-vibrational transition lines responsible for these features at 300 K is up to twice the intensity at 500 K.

6 CONCLUSIONS

The BYTe and 10to10 line lists appear to be validated in that we have detected previously known features at the correct wavelengths. In addition, we have found new absorption features and corrected features which had previously been mis-identified. The reasons for this are the high quality spectra used in this analysis, and the 10to10 line list, which is more complete at these temperatures than any previously available list. For example, the CH_4 laboratory line list used by B11 was made at 800 K and covered the spectral range 2000-5000 cm^{-1} (wavelengths $\geqslant$2.00 μm) at a resolution of 0.02 cm^{-1}, and the spectral range 5000-6400 cm^{-1} (wavelengths between 1.56-2.00 μm) at a resolution of 0.04 cm^{-1} (Nassar & Bernath 2003). B11 used the HITRAN 2008 database (Rothman et al. 2009), calculated at 296 K, to supplement the experimental line list. These facts may explain B11's mis-identifications, particularly in the J- and H-bands. The use of adaptive optics has enabled us to obtain data in the H- and K-bands with improved S/N ratios compared with the same passbands in B11. This has allowed us to add significantly to the number of detections of methane and ammonia absorption features in this region of the near-infrared. Our near-infrared spectrum of UGPS 0722 and that of B11 appear very similar and we have not found any sign of variability of features between the two spectra. As both data sets are independent, we are confident that these features are real.

The BYTe and 10to10 line lists indicates that NH_3 is the dominant opacity source between ∼1.233-1.266 μm in UGPS 0722, and we have tentatively identified several absorption features in this wavelength range in the T9's spectrum which may be due entirely to ammonia opacity. Our analysis using the 10to10 line list suggests that water rather than methane is the dominant absorber in the red half of the J-band in 2MASS 0415, where water opacity is between 40-80% stronger than methane opacity. In UGPS 0722, water is the major opacity source until ∼1.31 μm when methane opacity starts to dominate. This result can be examined when the 10to10 line list is included in a full model atmosphere.

The 10to10 line list has allowed us to accurately identify the opacity sources responsible for many of the T dwarf absorption features. We have also found that absorption features common to both T dwarf standards may have different opacity sources, or the relative strengths of the opacity sources producing these features may vary between them. This is particularly noticeable in the J-band, where the number of absorption features due solely to CH_4 opacity is fewer than previously thought.

Using the high quality spectra of these T dwarfs, we

Table 11. Accuracy of the 10to10 line list in the H-band

Vibrational band	$\Delta\Gamma$	Accuracy, $\lambda(\mu m)$
$2\nu_3$	$F_1 \rightarrow F_2$	$\sim 2\times10^{-6}$
$2\nu_3$	$E \rightarrow E$	$\sim 8\times10^{-5}$
$2\nu_2 + \nu_3$	$F_2 \rightarrow F_1$	$\sim 1\times10^{-4}$
$\nu_3 + 2\nu_4$	$F_1 \rightarrow F_2$	$\sim 6\times10^{-3}$
$\nu_3 + 2\nu_4$	$F_2 \rightarrow F_1$	$\sim 8\times10^{-3}$
$\nu_1 + \nu_3$	$F_1 \rightarrow F_2$	$\sim 6\times10^{-3}$
$\nu_1 + 2\nu_2$	$A_2 \rightarrow A_1$	$\sim 8\times10^{-3}$

have been able to confirm the presence of 15 of the 19 NH_3 absorption features in the K-band predicted by the S12 models. In addition, we have identified six previously unknown absorption features. The ro-vibrational transition lines responsible for these features have up to twice the intensity of those in the H-band. The lines also appear to be more highly ordered than those in the J- or H-bands, making the identification of corresponding absorption features in the T dwarfs' spectra easier. We think that the conspicuous peaks of NH_3 opacity in the K-band are due to the strong transition dipole of the stretching mode of the $\nu_1 + \nu_4$ band. The stretching mode (ν_1) makes the strongest contribution to the ro-vibrational transition lines in this wavelength region. There are also no issues with forbidden bands, since the ammonia molecule has a permanent dipole. The $\nu_1 + \nu_4$ band has a transition dipole moment of 0.017 Debye. This compares with a moment of 0.0005 Debye for the $3\nu_4$ band, the band nearest in strength to the $\nu_1 + \nu_4$ band at these wavelengths.

In this work we have looked at the most common isotopologues of methane and ammonia. In particular, the relative abundance of methane isotopologues is determined by the reaction rates of these isotopologues with methane sinks (Rigby et al. 2012), and is therefore useful in understanding the structure and evolution of atmospheres. The use of high-temperature line lists of other methane isotopologues in model spectra could be applied to the near-infrared spectra of T dwarfs and would allow a greater understanding of the evolution of their atmospheres.

ACKNOWLEDGEMENTS

This paper is based on observations obtained in programmes GN-2010B-Q-18 and GN-2012B-Q-62 at the Gemini Observatory, which is operated by the Association of Universities for Research in Astronomy Inc., under a cooperative agreement with the NSF on behalf of the Gemini partnership: The National Science Foundation (USA), the Science and Technology Facilities Council (UK), the National Research Council (Canada), CONICYT (Chile), the Australian Research Council (Australia), CNPq (Brazil) and CONICET (Argentina).

J. I. Canty is supported by a University of Hertfordshire PhD studentship. Sergei Yurchenko and Jonathan Tennyson acknowledge support by ERC Advanced Investigator Project 267219 and the UK Science and Technology Research Council (STRC).

The authors are grateful to Didier Saumon for his numerous helpful comments.

REFERENCES

Bailey, J., & Kedziora-Chudczer, L. 2012, MNRAS, 419, 1913
Barber, R. J., Tennyson, J., Harris, G. J., & Tolchenov, R. N. 2006, MNRAS, 368, 1087
Bochanski J. J., Burgasser A. J., Simcoe R. A., West A. A., 2011, AJ, 142, 169 [B11]
Burgasser, A. J., Kirkpatrick, J. D., Brown, M. E., et al. 2002, ApJ, 564, 421
Delorme, P., Delfosse, X., Albert, L., et al. 2008, A & A, 482, 961
Cushing, M. C., Rayner, J. T., & Vacca, W. D. 2005, ApJ, 623, 1115
Cushing, M. C., Roellig, T. L., Marley, M. S., et al. 2006, ApJ, 648, 614
Cushing, M. C., Kirkpatrick, J. D., Gelino, C. R., et al. 2011, ApJ, 743, 50 [C11]
De Buizer, J., & Fisher, R. 2005, High Resolution Infrared Spectroscopy in Astronomy, 84
Dupuy, T. J., & Liu, M. C. 2012, ApJS, 201, 19
Dupuy, T. J., & Kraus, A. L. 2013, Science, 341, 1492
Fegley, B., Jr., & Lodders, K. 1996, ApJL, 472, L37
Freedman, R. S., Marley, M. S., & Lodders, K. 2008, ApJS, 174, 504
Geballe, T. R., Saumon, D., Golimowski, D. A., et al. 2009, ApJ, 695, 844
Hill, C., Yurchenko, S. N., & Tennyson, J. 2013, Icarus, 226, 1673
Irwin, P. G. J. 2003, Giant planets of our solar system : atmospheres, compositions, and structure, by P.G.J. Irwin. Springer Praxis books in geophysical sciences. Berlin: Springer, 2003
Lawrence, A., Warren, S. J., Almaini, O., et al. 2007, MNRAS, 379, 1599
Leggett, S. K., Saumon, D., Marley, M. S., et al. 2012, ApJ, 748, 74
Liu, M. C., Delorme, P., Dupuy, T. J., et al. 2011, ApJ, 740, 108
Lucas, P. W., Tinney, C. G., Burningham, B., et al. 2010, MNRAS, 408, L56

McGregor, P. J., Hart, J., Conroy, P. G., et al., 2003, Proceedings of the SPIE, 4841, 1581-1591
Mainzer, A. K., Roellig, T. L., Saumon, D., et al. 2007, ApJ, 662, 1245
Morley, C. V., Fortney, J. J., Marley, M. S., et al. 2012, ApJ, 756, 172 [M12]
Nassar, R., & Bernath, P. 2003, JQSRT, 82, 279
Noll, K. S., Geballe, T. R., Leggett, S. K., & Marley, M. S. 2000, ApJL, 541, L75
Oppenheimer, B. R., Kulkarni, S. R., Matthews, K., & Nakajima, T. 1995, Science, 270, 1478
Rayner, J. T., Toomey, D. W., Onaka, P. M., et al. 2003, PASP, 115, 362
Richard, C., Gordon, I. E., Rothman, L. S., et al. 2012, JQSRT, 113, 1276
Rigby, M., Manning, A. J., & Prinn, R. G. 2012, Journal of Geophysical Research (Atmospheres), 117, 12312
Roellig, T. L., Van Cleve, J. E., Sloan, G. C., et al. 2004, ApJS, 154, 418
Rothman, L. S., Gordon, I. E., Barbe, A., et al. 2009, JQSRT, 110, 533
Rothman, L. S., Gordon, I. E., Babikov, Y., et al. 2013, JQSRT, 130, 4
Saumon D., Geballe T. R., Leggett S. K., Marley M. S., Freedman R. S., Lodders K., Fegley B., Jr., Sengupta S. K., 2000, ApJ, 541, 374
Saumon, D., Marley, M. S., Cushing, M. C., et al. 2006, ApJ, 647, 552
Saumon, D., Marley, M. S., Leggett, S. K., et al. 2007, ApJ, 656, 1136
Saumon D., Marley M. S., Abel M., Frommhold L., Freedman R. S., 2012, ApJ, 750, 74 [S12]
York, D. G., Adelman, J., Anderson, J. E., Jr., et al. 2000, AJ, 120, 1579
Simcoe, R. A., Burgasser, A. J., Bochanski, J. J., et al. 2010, Society of Photo-Optical Instrumentation Engineers (SPIE) Conference Series, Vol. 7735
Skrutskie, M. F., Cutri, R. M., Stiening, R., et al. 2006, AJ, 131, 1163
Tennyson, J., & Yurchenko, S. N. 2012, MNRAS, 425, 21
Wenger, C., & Champion, J. P. 1998, JQSRT, 59, 471
Wright, E. L., Eisenhardt, P. R. M., Mainzer, A. K., et al. 2010, AJ, 140, 1868
Yurchenko, S. N., Barber, R. J., & Tennyson, J. 2011, MNRAS, 413, 1828
Yurchenko, S. N., & Tennyson, J. 2014, MNRAS, 440, 1649
Yurchenko, S. N., Tennyson, J., Bailey, J., Hollis, M. D. J., & Tinetti, G. 2014, Proc. Am. Acad. Sci., 111, 9379
Zapatero Osorio, M. R., Martín, E. L., Béjar, V. J. S., et al. 2007, ApJ, 666, 1205